Design an irreversible electroporation experimental apparatus: An approach to estimate and optimize the IRE dose

J.P. (Joao) Almeida

MSc Report

Committee:
dr.ir. M. Abayazid
G. Wardhana, MSc
dr.ir. J.F. Broenink
dr.ir. R. Hagmeijer

June 2019

022RAM2019
Robotics and Mechatronics
EE-Math-CS
University of Twente
P.O. Box 217
7500 AE Enschede
The Netherlands

Summary

Pancreatic adenocarcinoma is one of the leading causes of cancer-related deaths in occidental countries. The options for the treatment of pancreatic cancer that are currently available are limited, with surgical resection remaining as the only curative method. Still, the survival rates for patients that undergo surgery are very low.

Irreversible Electroporation (IRE) is an emerging technique that has drawn attention in the field of cancer treatment. By inserting electrodes in soft tissue, pulsed electrical fields are delivered to the cells, creating lethal nanopores in the plasma membrane to induce cell death.

There are several parameters that may influence the outcomes of IRE for a given tissue organ type. These parameters establish the IRE dose of the treatment. However, the application of this technique may result in undesired thermal damage of the tissue if the correct doses are not administered. In fact, the optimal combination of parameters is still unknown, whereby the efficiency of this technique can still be improved.

As a result, the optimal IRE dose for pancreatic cancer is investigated in this project. Parameters such as the number of delivered pulses, their amplitude and width were adjusted. In addition, the influence of the distance between the inserted electrodes and their active length were also studied.

2D simulation models were created to evaluate IRE outcomes such as the generated electric field and temperature changes in the tissue. Experiments were conducted using bovine liver tissue to measure the temperature increase during IRE. The temperature measurements obtained from the experiments were then used to validate the results obtained from the simulation models.

The models were successfully validated for biological tissue when the electrodes were inserted in the tissue separated by distances between 10 and 20 mm. Furthermore, statistical analysis revealed significant influence of the distance between the electrodes, the pulse width and the voltage on the temperature achieved in the tissue after IRE.

Once validated, optimization of the IRE dose was done for the treatment of pancreatic cancer. The optimal dose was calculated using data from the validated models. The optimal parameters produced an electric field magnitude of 3296.1 V/cm between the electrodes and a maximum temperature of 46.796°C in the tissue surface. No thermal damage in pancreatic tissue is expected after applying an IRE treatment with this optimal dose.

Preface

First, I would like to thank my parents, my brother and my grandparents for all the support they gave me during my thesis and for being there, all the time, in the good and bad moments of my life.

I would like to express my sincere gratitude to my supervisor, dr. Ir. Momen Abayazid for all his support and availability during the realization of my project. Whenever I had a question or needed some guidance his office door was always open.

Special thanks also to dr. Mohammed Shurrab who guided me during the first part of my thesis and to Giri for meeting me regularly to discuss the progress of my thesis.

I would also like to thank dr. Ir. Jan Broenink and dr. Ir. Rob Hagmeijer for accepting being members of my committee.

A special acknowledgement to Henny who contributed so much for the detailed process of designing and building my experimental apparatus. His help was fundamental for the project. Also, thanks to the other technicians Gerben, Marcel and Sander for the help during the experimental part of my thesis.

A special word to Hamid for helping me with the simulation models and to prof Gijs Krijnen for meeting me to clarify some ideas.

I would also like to thank Jolanda for all the support with the paperwork and logistics of my thesis.

A special word for all my fellow colleagues of the Medical Robotics Subject Group who gave feedback about my project and for the good environment during the biweekly meetings.

Last but not least, a special acknowledgement for all my friends here in Enschede: Anas, Antonio, Estima, Hannah, Larraitz, Maria, Pedro, Sora and Tony. A special thanks for all you guys who stand next to me during this amazing journey here in this little corner of the eastern Netherlands.

João Pedro
Enschede, 24 June 2019

Contents

1 Introduction

1.1 Context

Pancreatic adenocarcinoma is the most common malignancy of the pancreas and one of the leading causes of cancer-related deaths in occidental countries [1, 2]. The early symptoms of pancreatic cancer are usually uncertain and mild, therefore the diagnosis of pancreatic cancer is obtained at a late stage, when the tumors are already at an advanced stage and starting to spread outside the pancreas to the nearby organs and vessels [3]. As a result, around 30% of patients with pancreatic cancer present with Locally Advanced Pancreatic Carcinoma (LAPC) [4].

The available options for the treatment of pancreatic cancer are scarce, with surgical resection remaining as the only curative method [5]. However, most LAPC patients present with unresectable disease due to the advanced stage of the tumors [5]. Surgical resection can only be performed in 15% of the patients that suffer from pancreatic cancer and still the survival rate for these patients is very low, presenting a 5-year-survival rate of approximately 20% [1]. For the remaining 85%, the 5-year survival rate of unresectable patients drops down to extremely low values, less than 5% [1, 6].

Unresectable LAPC patients are usually recommended with additional chemotherapy and radiotherapy treatments as an attempt to reduce the tumors to a point where resectability is restored. Nevertheless, the outcomes of these treatments are still far from being satisfactory [2, 5, 7].

Minimally invasive techniques for cancer ablation have arisen as an alternative for the treatment of pancreatic cancer. These techniques would allow the treatment of primary tumors without performing surgery, providing an effective treatment with a smaller impact on the patient. Some of these techniques have been studied for the treatment of pancreatic cancer. Thermal ablation methods such as Cryoablation, Radiofrequency Ablation (RFA), High-Intensity Focused Ultrasound (HIFU), Laser Ablation and Microwave Ablation have shown to be applicable and safe [8]. Unfortunately, these methods suffer from a major flaw. Their main principle is based on the necrosis of tumor cells due to the use of thermal energy, a process that may damage major structures that surround the pancreas, such as the superior mesenteric artery, the portal vein, and the common bile duct (Figure 1.1). In addition, the proximity of the pancreas to these two large blood vessels may induce the heat-sink effect, in which the blood flow cools down the adjacent tissue leading to an ineffective ablation of the malignant cells [5, 9].

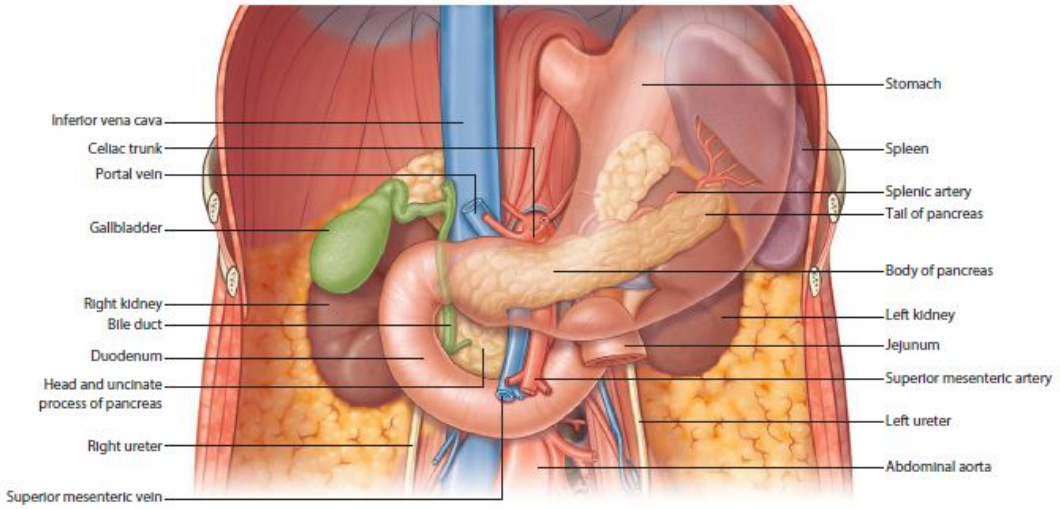

Figure 1.1: Pancreas and related structures [10]

Irreversible Electroporation (IRE) is a minimally invasive surgical procedure that has drawn interest in the field of focal cancer ablation over the last decade. The electroporation technique consists in the exposure of cells to strong electric fields delivered by electrodes inserted in the soft tissue. This process causes an electrical breakdown of the membrane and increases its electric conductivity and permeability [11]. If the applied electric field is strong enough, electroporation can be irreversible, which is characterized by the irreversible generation of nanopores in the plasma membrane leading to eventual cell death by apoptosis and necrosis [5, 11]. Apoptosis is the natural process of cell death and it usually allows the regeneration of the treated tissue. On the other hand, necrosis is a form of cell injury that leads to the formation of fibrotic scar tissue. An advantage of IRE over thermal methods is that it is believed that cell death by apoptosis is relatively higher in IRE [5].

Theoretically, the process of tissue ablation generated by IRE can be assumed as non-thermal since it relies on electrical energy to disrupt the cell membrane [5]. This is a significant advantage when compared to the classic thermal methods that depend on thermal energy for the same purposes. As a result, IRE has the potential to be applied in areas of tissue that are located next to high-vascularized structures, as it is the pancreatic case, without compromising the vessels or inducing the heat-sink effect [5].

1.2 Problem Statement and Motivation

The application of electric fields in tissue may produce several phenomena simultaneously. Recent studies have shown that despite IRE is considered a non-thermal method, the application of this technique may result in Joule heating of the tissue [12, 13, 14]. Joule heating is described by the conversion of the energy of an electric current that flows through a resistance into heat. During IRE, some of the electrical energy that is delivered to the cells is usually converted into thermal energy, increasing the temperature. If it exceeds a certain threshold, undesired thermal damage of the tissue may occur. Thermal damage begins at temperatures around 42°C if the exposure to the treatment is long (seconds to hours of exposure). The rate of damage drastically increases around 50°C - 60°C [15]. Therefore, it is assumed that temperatures above 50°C are likely to cause thermal damage in the tissue [5].

Several parameters can have influence on the outcomes of an IRE treatment on a certain tissue organ type. These parameters establish the IRE dose of the treatment, and they are mostly related to the pulses that are delivered to the cells and to the configuration of the inserted elec-

trodes. Depending on the applied dose on the procedure, the electric field generated in the tissue and the consequent temperature results will diverge. As a result, by varying some of these parameters, it can be possible to reduce the thermal effect caused by Joule heating without compromising the ablation process.

Optimization of the IRE dose is therefore essential to avoid thermal damage of vital structures of the body. Nevertheless, the optimal combination of parameters is still unknown, whereby there is still room for improving the efficiency of the IRE methodology.

1.3 Research Question

In order to overcome the limitations addressed in the previous section, one question stands out: **What can we do to optimize the outcomes of an IRE procedure?**

As a result, the main goal of this project consists in presenting the optimal IRE dose for pancreatic cancer. To provide concise answers regarding this matter it is important to assess the thermal effects that may result from an IRE procedure in order to find the combination of IRE parameters that would maximize the efficacy of the treatment and minimize the thermal damage in the tissue.

1.4 Methodology

To achieve the goals proposed in this project, two-dimensional simulation models were created to enable the study of electric field and temperature distributions and in the tissue and their changes during IRE, according to the chosen parameters. The results obtained from the models were validated experimentally. An experimental setup was built to perform the experiments in bovine liver tissue. When validated, a statistical analysis of the obtained results from simulation was performed. The ANOVA test was applied to study the significance of the different parameters on the IRE responses. Lastly, and assuming that the models were validated for biological tissue, the electrical and thermophysical parameters of pancreatic tissue were introduced. Optimization was performed using Response Surface Methodology.

1.5 Outline of the Report

This report unfolds as the following. The current chapter introduces the clinical problem and IRE as a potential treatment, presenting the motivation and the aims of the present study. Chapter 2 is mostly informative, presenting an overview of the electroporation topic with a focus on the IRE method. In Chapter 3, a comprehensive review of studies regarding the optimization of the IRE methodology and the clinical application of IRE in pancreatic cancer is provided to the reader. The 2D numerical models and the experiments performed with bovine liver are described in Chapter 4. In Chapter 5, the results obtained from both simulation models and experiments are compared for model validation. Chapter 6 provides the optimal IRE dose for pancreatic cancer. Discussion of the obtained results is presented in Chapter 7. The conclusions and suggestions for future research can be found in the seventh and final chapter of this report.

2 Background

Electroporation is a phenomenon in which cells are exposed to short and intense electric field pulses, increasing the permeability of the plasma membrane. Depending on the duration and the intensity of the applied fields, electroporation can be either reversible or irreversible.

IRE has received interest for soft tissue ablation procedures. This technique can still be optimized through the variation of certain parameters regarding the delivered pulses and the electrodes that are used.

This chapter provides a wider perspective on irreversible electroporation. Section 2.1 describes the events that occur during electroporation at a cellular level. Section 2.2 presents some IRE applications. Section 2.3 presents the materials and equipment. Finally, Section 2.4 discusses the outcomes of this technique.

2.1 The Electroporation Phenomenon

The application of external electric fields in soft tissue increases the permeabilization of the plasma membrane. This phenomenon is called electroporation or electropermeabilization [16].
Although there are still some biophysical events at the membrane level that are not fully understood, it is consensual that electroporation can be described by the theory of aqueous pore formation [11]. According to this theory, the application of an electric field on the tissue modifies the transmembrane potential of the cells, inducing a voltage across the membrane. Consequently, the energy required for the spontaneous formation of aqueous pores in the phospholipid bilayer is reduced, resulting in the formation of a larger number and more stable pores (Figure 2.1) [5, 11].

If the exposure time of the cell to the electric field is short enough, or if the intensity of the electric field is not high enough, the membrane is able to recover. In this case, the electroporation is reversible [11]. Nevertheless, the process of membrane recovery is not completely understood, and it is still a matter of study [17].

On the other hand, electroporation can be irreversible when the tissue is exposed to very intense electric fields, or when the exposure time is long enough. It is considered that the threshold for IRE is around 700 V/cm [18]. This extensive permeabilization of the membrane may result in cell death, due to a permanent membrane lysis or due to a loss of homeostasis (there is leakage of cellular contents and the cell loses stability) [11, 17, 19].

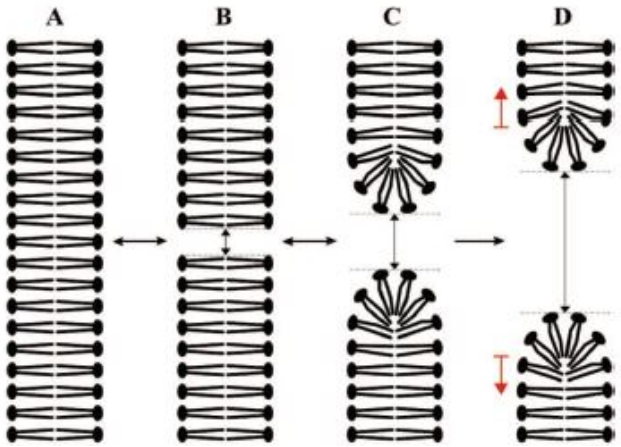

A: Bilayer without pores
B: Bilayer with a hydrophobic pore
C: Reversible transition of the membrane into a metastable hydrophilic pore
D: Irreversible transition of the membrane into an unstable self-expanding hydrophilic pore

Figure 2.1: Pore formation in the cell membrane (Adapted from [11])

2.2 Applications of IRE

IRE has gained interest in clinical medicine as a focal therapy for soft tissue ablation. Currently, it is being implemented on the treatment of advanced oncological diseases of the liver, lung, kidney, brain or pancreas [19, 20]. Technically, IRE is a simple and fast technique, keeping the advantage of being a minimally invasive procedure [19]. In addition, it has the advantage of allowing the use of conventional imaging modalities such as ultrasound, Computed Tomography (CT) or Magnetic Resonance Imaging (MRI) for guidance during the clinical procedure [16].

Irreversible electroporation is also being investigated in other study areas. In biotechnology, it has been used for the extraction of biomolecules and for microbial deactivation [19]. Other application areas of IRE include tissue engineering and regenerative medicine [5].

2.3 IRE: Materials and Equipment

IRE procedures involve two indispensable materials: electroporators and electrodes. The electroporator or pulse generator delivers pulsed electric fields to the tissue through the insertion of electrodes.

Electroporators

The electroporator device generates short High-Voltage (HV) pulses, allowing the user to specify their parameters, such as the shape, the amplitude, the duration of each pulse, the number of pulses and the frequency [21]. All these pulse parameters characterize the IRE signal and define the energy delivered to the tissue [21].

Typically, IRE protocols use series of square pulses [5]. It is relevant to mention some terminology related these waveforms. Regarding the polarity, they can be defined as monopolar or bipolar. If the amplitude of the pulse only varies positively, then the pulse is monopolar. On the other hand, if it varies in both positive and negative directions, the pulse is named as bipolar. The term pulse width usually refers to the time in which the pulse is "on". The inter-pulse delay can be defined as the time between pulses, this is, the spare of time that goes from the end of

a pulse until the onset of the following one. The intra-pulse delay is often used to describe the delay between pulses of opposite polarity in bipolar pulses. Figure 2.2 provides a schematic representation of the terms that were previously described.

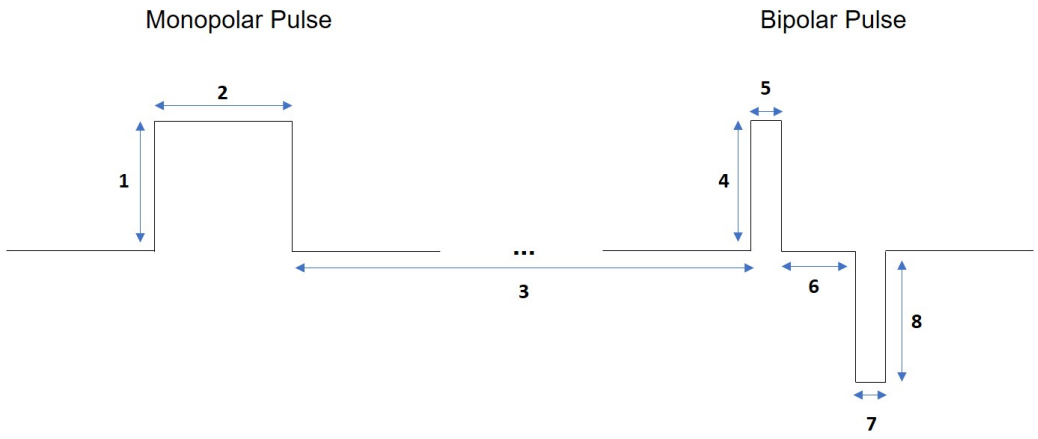

1: Amplitude
2: Pulse width
3: Inter-pulse delay
4: Positive amplitude
5: Positive pulse width
6: Intra-pulse delay
7: Negative pulse width
8: Negative amplitude

Figure 2.2: Bipolar and monopolar square pulses

Electrodes

In IRE a series of short HV pulses is generated by the electroporator and delivered to the tissue by electrodes that are placed around and/or inside the target tumor [5, 14]. Usually, the electrodes used for clinical practice and *in vivo* experiments are either needles or plates. Plate electrodes are applied for the treatment of superficial tissues, whilst needle electrodes are used to treat deeper tumors. If the volume of the tumor is considerable it is also possible to use a multiple-needle electrode configuration [21].

Needle electrodes are commonly made of stainless steel or titanium [21]. Usually, they are covered with an insulating material, except for a certain tip length. The length of the exposed tip is described as the "active tip length", and it is the interface that delivers the pulses to the soft tissue [22].

2.4 IRE: Outcomes

IRE is considered as a non-thermal ablation method. It relies on electrical energy to induce cell death therefore it can be applied to tumor treatment located in the immediate vicinity of vascular and heat-sensitive structures such as nerves or bile ducts without damaging them [5, 23, 24]. However, thermal energy is generated when electrical current travels through a resistive material [5]. This process is called Joule Heating. During an IRE procedure on biological tissue, electric current travels through the inserted electrodes, and part of the energy is delivered to the tissue as heat [5]. As a result, the temperature may increase to unsafe levels during the procedure, which can be harmful in the presence of thermally vulnerable structures [5, 14]. It is assumed that temperatures above 50°C may cause thermal damage in the tissue [5].

The ideal IRE treatment would consist in a complete coverage of the damaged tissue, applying sufficiently high electric fields in order to ablate it while guaranteeing, simultaneously, that the temperature increase during the procedure is not enough to generate thermal damage.

An analysis of the electric field and temperature responses is therefore fundamental since it can provide valuable information for improving the efficacy of the treatment. There are several parameters that may influence these responses. Varying pulse settings such as the shape of the pulse, the intensity, the number of delivered pulses, the duration and the frequency may produce considerable different results regarding the electric field, the temperature and the consequent volume of ablated tissue.

The distribution of the electric field also depends on the electrical conductivity of the tissue and on the positioning of the electrodes in the tissue. They should be placed parallel to each other so that the electric field is homogeneous [5]. Furthermore, electrode configurations such as their geometry, the number of inserted electrodes, the length of the electrode and the active tip length, the diameter and the separation between inserted electrodes may also influence the created field.

3 Literature Review

The optimal IRE dose for a determined tissue organ type depends on diverse parameters, mostly related to delivered pulses and inserted electrodes. Although several studies have investigated the influence of these parameters on the electric field and thermal responses of IRE, the optimal IRE dose is still unknown.

Section 3.1 of this chapter presents a comprehensive compilation of published studies related to the IRE method and the corresponding parameters. The papers included in this review used different types of research. Some papers show results obtained from numerical simulations while others present different experimental study types such as *in vitro*, *in vivo* or experiments performed in tissue phantoms. Nonetheless, all these papers present relevant results regarding the electric field and thermal effects of IRE, providing valuable information about the IRE parameters that are commonly established.

In the meanwhile, some medical procedures related to the treatment of pancreatic cancer using IRE have been performed with relative success. Section 3.2 presents an overview on clinical studies concerning the application of IRE in the treatment of pancreatic cancer. The information provided in this section gives insights about the state of the art of IRE in clinical practice for pancreatic applications.

3.1 IRE Studies

3.1.1 Simulation Studies

Simulation modeling is the process of creating and analyzing a mathematical model capable of predicting the performance of a system. A simulation model allows the engineer to analyse different phenomena occurring in a system and to help designing it, avoiding the repeated construction of physical prototypes to do so.

In IRE, simulation models can be important to predict heat transfer patterns and other underlying processes, as well as to evaluate the effect of several parameters in the electric field, temperature or cell ablation.

Davalos et. al (2005) were pioneers in proposing IRE as a technique capable of ablating considerable volumes of tissue, without causing any harmful thermal effects [15]. 2D mathematical models were created, simulating a typical electroporation procedure in the liver. Configurations of 2 electrodes with diameters of 0.5 mm, 1 mm and 1.5 mm were tested. For a separation of 10 mm, and a pulse width of 800 µs, it was found that the range of voltage at which the temperature reaches 50°C goes from 888 V with the 0.5 mm-diameter electrode to 1613 V with the 1.5mm-diameter electrode. In addition, results showed that the temperature increase is most pronounced on the electrode-interface, specifically in between the electrodes. Furthermore, it was found that varying the number of electrodes changes the shape and size of the ablated region.

In a following study, Davalos et. al (2008) evaluated the effects of typical IRE protocols in the temperature distribution through 2D numerical models of spherical and cylindrical electrodes [25]. 1000 V were applied across the electrodes. Results revealed that the field distribution strongly depends on the electrode shape. Spherical electrodes required less time to reach 50°C than cylindrical electrodes. Also, they concluded that both the electric field and temperature distributions decay more gradually in a cylindrical geometry than in a spherical one.

Garcia et. al (2014) investigated the probability of cell death due to IRE and thermal damage in a 2D liver model [14]. 90 pulses of 3000 V with a duration of 100 µs were delivered at a

frequency of 1 Hz. Numerical simulations of the electric field and temperature distributions were performed. The apparatus consisted in 2 cylindrical electrodes with a separation of 8 mm and length of 7 mm. Results from the simulations showed that cell death is a function of electric field strength and pulse number and there is a minimum number of pulses (40 pulses) and electric field intensity (500 V/cm) to achieve 99.9% probability of cell death. They also found that at 30 pulses thermal damage starts occurring around the electrodes and that at 90 pulses there is already significant damage in the tissue.

Latouche et. al (2015) did a 3D reconstruction of a tumor, healthy pancreatic tissue and vasculature structures from a pancreatic cancer patient [6]. The IRE dose consisted in 90 pulses with a strength of 3000 V and duration of 100 µs. Numerical simulations of the electric field and temperature distributions were made using a 2-electrode array, with 2 cm of separation and 1.5 cm exposure length. A maximum temperature of 38.65°C was measured at a center point between the electrodes, 7.5 mm from the tip along the exposed electrode.

Moser et. al (2018) studied the influence of electrode properties and pulse strength on the volume of ablated tissue and maximum temperature generated in a liver tissue [26]. Computational simulations in a 3D liver model were performed. 90 Pulses of 100 µs duration were delivered at a frequency of 1 Hz. Results from these simulations showed that the pulse strength has significant impact on both temperature and ablation volume. On the other hand, the electrode diameter had no significance in neither of them. In addition, the distance between electrode and center, and the number of electrodes had significant impact on the maximum temperature. The electrode length was significant only on the ablation volume. Results showed a maximum ablation volume of 1500 mm^3. Moreover, a maximum temperature of 53°C was achieved at a pulse strength of 2500 V.

This collection of simulation studies provide valuable insights about IRE parameters and the outcomes that depend on them. However, the translation of these studies into experiments would have helped to confirm the reliability of their findings. Furthermore, these simulation studies present useful results that should be taken into account before designing an experimental apparatus for IRE studies.

3.1.2 *In Vitro* Studies

In vitro studies are usually performed with microorganisms, cells, or biological molecules either in a test tube or laboratory dish. As a result, these studies allow researchers to grow cells independent of the body, providing a simple and convenient way to perform IRE experiments without using the whole organism.

Bischof et. al (2013) made an *in vitro* experiment to test membrane-targeting approaches in order to increase the ability of IRE to destroy undesirable cells [24]. One of these approaches is the so-called pulse delivery timing method: here, 51 pulses were divided into 3 trains of 17 pulses each, with varied delays between trains (10 s, 30 s, 1 min, and 2 min). The *in vitro* experiment was conducted in an electroporation cuvette, whose plates had a 2 mm separation, placed in an external electric field of 1000 V/cm. Each pulse had a strength of 200 V, 50 µs duration and a frequency of 10 Hz. Results showed a 67% increase in cell destruction compared to a baseline IRE dose. Regarding temperature, pulse timing reduced the maximum temperature rise to less than 1°C.

A study conducted by Shao et. al (2018) investigated pulse timing as a physical IRE enhancement approach [27]. The pulse delivery scheme consisted in 51 pulses divided into 3 trains of 17 pulses each, with 30 s delay between them. The *in vitro* experiment was done on a cell suspension of pancreatic cancer cells, using 2 plate electrodes with a 2 mm separation. Results

showed a viability drop of 5-10% in pulse timing in comparison to the baseline group. The study did not test the temperature outcomes.

Zhang et al. (2018) studied different pulse delivery schemes through an *in vitro* experiment [28]. Three different combinations of pulses were considered: 2x45 pulses, 3x30 pulses and 5x15 pulses with 10 s, 30 s and 60 s delays between each series. The pulse repetition rate was another parameter that was investigated: pulse repetition rates of 1 pulse per 200 ms (5 Hz) and 1 pulse per 550 ms were tested. The pulse strength was 1000 V and each pulse had a duration of 90 µs. In this experiment, two needle electrodes separated by 5 mm, and with a total length of 5 mm were inserted in a potato, with an insertion depth of 22 mm. Temperature was measured using a commercial temperature probe that was inserted into one of the insertion holes of IRE electrode. No lethal temperatures superior to 50°C were recorded. The largest ablation volume obtained at a 200 ms rate was 1634.1 mm^3 using a pulse delivery scheme of 2x45 pulses with 10 s delays. At 550 ms rate, the maximum volume of ablated tissue was 1828.4 mm^3, considering 2x45 pulses with 60 s delays.

These *in vitro* studies are useful in the way that they provide insights on how cells of different tissues react to IRE treatments. Nevertheless, it would have been convenient if some of these studies were replicated into *in vivo* studies, like it was done by Bischof et al., in order to predict the reaction of an entire organism to IRE treatments.

3.1.3 *In Vivo* Studies

In vivo studies are usually performed on living organisms, such as laboratory animals or humans. In some cases, *in vitro* studies might present promising results that are not corroborated by subsequent *in vivo* experiments. Therefore, these studies are important in order to assess how the body would respond to the application of a certain IRE treatment.

Bischof et. al (2012) investigated the electrical and thermal effects of IRE in prostate cancer cells grown *in vivo* in a thin 2D Dorsal Skin Fold Chamber (DSFC) [29]. 10, 50 or 99 pulses of 500 V were delivered at a frequency of 10 Hz. The duration of each pulse was also varied (10, 50 or 100 µs). The experimental setup included a needle electrode in the center, surrounded by 1 ring electrode. An infra-red camera was used to record temperature changes from above the tumor. The maximum temperature change recorded by the camera was 19±2°C, using an IRE dose of 99 pulses with duration of 100 µs.

Bischof et. al (2013) also made an *in vivo* experiment to test the pulse delivery timing method in IRE [24]. The experiment was performed on a 2D DSFC. 51 pulses were divided into 3 trains of 17 pulses each, and each pulse had a strength of 500 V and a duration of 50 µs. Electrical and thermal models were used in numerical simulations. The apparatus consisted in a needle electrode placed in the center and surrounded by a ring electrode. Results from the simulations presented a maximum electric field intensity of 4000 V/cm and a maximum temperature of 39.5°C, calculated around the needle electrode. An infra-red camera was placed above the tumor to record the temperature experimentally. However, no experimental data regarding temperature was presented in the study.

In a following study, Bischof et. al (2014) created a 3D human prostate cancer model *in vivo* to verify that pulse timing can be applied for the treatment of larger volumes of tumors, without causing thermal injury [23]. 51 pulses were divided into 3 trains of 17 pulses each, with 30 s delay between them. Each pulse had an intensity of 600 V, duration of 50 µs and frequency of 10 Hz. Numerical simulations of the electric field and temperature distributions were made using 2D models. Two needle electrodes were used, with a separation of 4 mm and an insertion depth of 3 mm. Simulation results displayed a maximum electric field intensity of 3618.8 V/cm and a maximum temperature of nearly 43°C, calculated next to the inner side of the electrodes.

Experimental results showed that pulse timing achieved 33% more tumor volume ablated than baseline IRE.

Dunki-Jacobs et. al (2014) assessed potential thermal injuries during IRE in *in vivo* porcine models of liver, pancreas and kidney tissue [12]. 90 Pulses of 3000 V were delivered with a duration of 70 µs or 100 µs each.The experiment used two needle electrodes separated by 2 cm and with variable exposure lengths of 1.5, 2 or 3 cm. Two thermocouples were used to measure temperature and they were placed between the electrodes at 0.5 cm and 1 cm distance from one of the electrodes. The greatest increases in temperature were found at the thermocouple placed within 0.5 cm for all cases. For pancreatic tissue, the mean maximum temperatures found were 51°C and 46.3°C for the 0.5 cm and 1 cm thermocouple distances, respectively. In addition, results regarding the pancreatic tissue showed that to avoid thermal injury, it is advisable to use a maximum active length of 1.5 cm, a maximum pulse width of 90 µs and a distance of 1.5 cm to 2.3 cm between electrode pairs.

Shao et.al (2018) did an *in vivo* experiment to study pulse timing as an IRE enhancement method by injecting cancer cells in mice [27]. The delivered pulses had a strength of 600 V, duration of 50 µs and frequencies of 10 Hz or 1 Hz. The IRE apparatus consisted in 2 needle electrodes, separated by 4 mm and with an insertion depth of 3 mm. The electric field distribution was evaluated through a 2D simulation. Pulse timing led to 32%-45% smaller tumor volumes. In addition, this study provided the first evidence of adaptive resistance to IRE in pancreatic cancer cells. However, this study did not provide information about temperature.

3.1.4 Tissue Phantom Studies

Tissue phantoms are composed of tissue-mimicking materials to research phenomena *in vitro* and predict *in vivo* effects. By applying an IRE treatment to a certain tissue phantom, it should respond in a similar manner to the human tissue or organ that it represents.

Yao et. al (2017) investigated a different pulse delivery approach: Synergistic High and Low-Voltage Pulses (SHLVP), in which short high-voltage pulses were applied in a potato tissue phantom, followed by long low-voltage pulses [30]. The experiment used 8 needle electrodes (4 parallel pairs) with a separation of 2.5 mm between positive and negative electrodes and 2 mm between electrodes with the same polarity, and an insertion depth of 6 mm. Temperature was measured with fiber optic sensors at two different points between the positive and the negative electrodes. The maximum temperature difference recorded was 1.1°C. Results also showed higher ablation volumes when using this synergetic pulse combination.

Nevertheless, it is required more information about the use of potatoes as tissue phantoms in IRE. It is important to know if a potato tissue phantom can represent the properties of human tissue accurately.

Furthermore, the use of tissue phantoms to simulate IRE procedures still requires some research. Finding the correct materials to form a tissue phantom capable of mimicking a specific human tissue can be an useful tool to reproduce the phenomena that could happen in the human body during an IRE procedure.

3.2 IRE in Clinical Practice

3.2.1 NanoKnife

First introduced to the US market in 2007, the NanoKnife system has been used in more than 5450 clinical procedures [31]. Until now, it is the only available IRE system that has been approved for clinical use [22].

The NanoKnife apparatus contains a pulse generator that can deliver series of 10 to 100 pulses with amplitudes up to 3000 V and durations in the range of 20 to 100 µs. IRE can be delivered using arrays of up to 6 electrodes. The electrodes present a trocar tip for better tissue penetration. Furthermore, the system allows the user to manually adjust the active tip length from 0 to 25 mm [22].

The NanoKnife system also includes a graphical interface that displays a simulation of the ablation area according to the treatment settings defined by the user [5]. However, the NanoKnife is not capable of reporting the energy applied in each treatment [22].

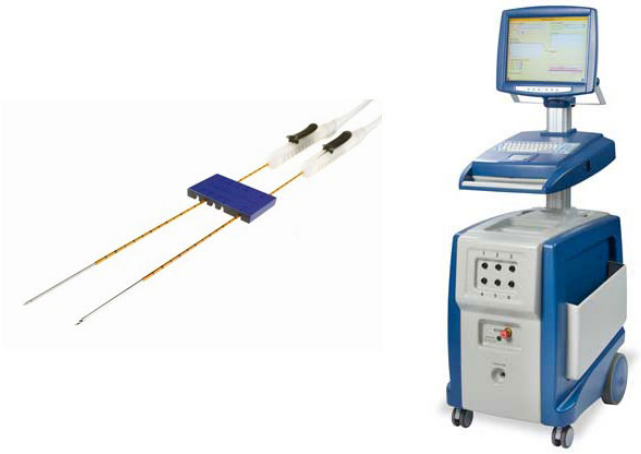

Figure 3.1: The NanoKnife system

3.2.2 Clinical Studies on Pancreatic Cancer

Some clinical procedures have already been performed in human pancreatic tissue. Results confirm the possibility of applying IRE treatments with relative safety and efficacy. Nevertheless, some adverse events do still occur to some patients who received treatment.

The treatment of pancreatic cancer through IRE can be performed in two different ways: percutaneously or through an open approach. Percutaneous IRE has the advantage of being a less invasive method than open IRE and it can be image-guided during the procedure. On the other hand, open IRE can differentiate between resectable and unresectable tumors in real-time and also detect metastases that might be present and are not visible through imaging [5].

Martin et al. (2012) reported the first study regarding the use of an IRE treatment in human pancreatic cancer, a prospective multi-institutional pilot evaluation of 27 LAPC patients undergoing open IRE [32]. The IRE treatment was delivered using the NanoKnife system. 2 probes with 2 cm distance and 1.5 cm active length were used. The delivered pulses had a pulse width of 100 µs and generated 1500 V/cm. Information about the pulse repetitions was not provided in the paper. Apart from a single mortality case, no other postoperative complications were registered, and all the patients who completed the 90-day follow-up period underwent successful ablation of all tumors.

In a following study, Martin et al. (2013) reported a study in which 54 unresectable LAPC patients underwent through an IRE procedure successfully, showing improved overall survival results in comparison with the standard chemoradiation-chemotherapy treatments [33]. The NanoKnife was the system used to deliver the treatment, and the IRE protocols were identical to the ones applied in their previous study.

Narayanan et al. (2012) evaluated the safety of percutaneous IRE in 11 LAPC patients with unresectable disease [7]. The NanoKnife system delivered 90 pulses of 70 µs pulses and intensities

varying between 1500 V and 3000 V. Two electrodes were inserted in the tissue with a separation of 2.2 cm. The study does not mention the active length of the electrodes. Results showed that there were no patients suffering from serious adverse events and there were either no deaths resultant from the IRE procedure.

Bagla and Papdouris (2012) performed a single-case study in a 78-year old patient with unresectable pancreatic adenocarcinoma [34]. A treatment with percutaneous IRE was applied to the patient using the NanoKnife system. Four electrodes with 1 cm active length were inserted in the tumor with an average spacing of 1.8 cm. 90 pulses were delivered but the authors do not detail information such as the magnitude of the pulses and the pulse width. Results showed successful ablation of the tumor with no recurrence.

In a study conducted by Paiella et al. (2015), ten unresectable LAPC patients received successful pancreatic IRE treatment, yet two IRE-related complications were registered in one patient [2]. Six probes of the NanoKnife apparatus were inserted in the tumor and spaced between 1 and 2 cm. There is no reference about the active length of the electrodes. The 90 delivered pulses had 70 µs width and generated at least 1500 V/cm in the tissue.

These clinical studies provide an overview on how IRE is being applied for the treatment of pancreatic cancer. The NanoKnife is the electroporation system used in clinical practice and the applied protocols have produced satisfactory and promising results. Therefore, the parameters used in these protocols and their range of values should be taken into consideration when designing IRE studies.

4 Experiments and Simulation Models

Initially, IRE experiments were planned to be performed in a gelatin tissue phantom that could mimic the properties of biological tissue. However, it was not possible to successfully perform the experiments with the prepared gelatin (see Appendix A).

As a result, IRE experiments were conducted in *ex vivo* bovine liver tissue instead. *Ex vivo* experiments allow to study the outcomes of an IRE procedure in the tissue of an organism in an external environment that can reproduce natural conditions.

Trains of monopolar HV pulses were delivered to bovine liver tissue through the insertion of two cylindrical electrodes. These pulses were generated by a pulse generator device: the Gemini X2 electroporator. The shape of the pulses was defined as monopolar squared pulses taking into account the settings of this device.

Several combinations of parameters were tested in the experiments. These parameters include the active length of the electrodes, the distance between the electrodes, the amplitude of the delivered pulses, the width and the number of pulses. Temperature changes in the tissue during the experiments were the measured responses.

In addition, mathematical models were computed to simulate the IRE experiments and to obtain the expected temperature responses. After, the results obtained from the experiments will be compared to the results obtained from simulation in order to validate the models for biological tissue.

The first section of this chapter describes the design of the experiments, as well as the experimental setup along and the followed procedure. Section 4.2 presents the simulation models that were built, making reference to the mathematical models that were used and the electrical and thermophysical properties of the different materials.

4.1 Experiments

4.1.1 Design of Experiments (DOE)

Different IRE protocols were designed to test distinct combinations of parameters. Five parameters were tested in different levels. The term levels is related to the number of different values that a variable can assume. The values were chosen taking into account the protocols that are currently used in clinical practice.

The distance between electrodes, the applied voltage, the number of pulse repetitions and the pulse width were four studied parameters and they were evaluated in three levels. This way, it was possible to study low, medium and high values of each parameter. The active length of the electrodes is another parameter that was considered but it was tested only in two different levels (low and high) for the sake of reduction of the number of experiments to perform.

All these parameters are thought to influence the temperature outcomes of an IRE procedure [12, 26]. Therefore, experiments were conducted to evaluate the influence of each one of them. Table 4.1 presents the different levels of the parameters that were considered for this study. In Figure 4.1, a scheme of the inserted electrodes is depicted.

Level	Active Length (mm)	Distance Between Electrodes (mm)	Input Voltage (V)	Pulse Repetitions	Pulse Width (µs)
1	10	5	500	40	40
2	15	10	1500	80	70
3	-	20	3000	90	100

Table 4.1: Levels of the tested parameters

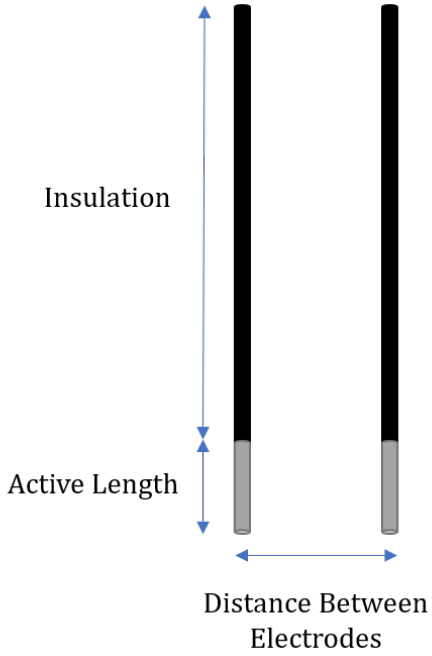

Figure 4.1: Configuration of the electrodes

The diameter of the electrodes and their length were not varied in this study. Evidence from literature statistically showed that both factors had no significant impact on the temperature results [26]. Therefore, they were defined as 1 mm and 15 cm, respectively.

The frequency of the pulse trains was defined as 1 Hz. In fact, Shao et. al found that a reduced frequency can enhance cell death by IRE at a certain electric field [27]. Consequently, one square pulse was delivered every second of the experiment.

Factorial Design

A factorial design consists of an experiment whose design has two or more independent variables (factors) that can assume a certain number of possible values (levels) [35]. This design allows the study of the main effects of each factor on the dependent variable and also the effects of interactions between factors on the dependent variable.

According to Table 4.1, with four factors assuming three different levels and another factor with two levels it would possible to make 162 different combinations of parameters. However, since this is not a reasonable number of experiments to be conducted, the Taguchi method was applied to reduce them.

Taguchi Method

Genichi Taguchi was famous for developing methods of robust quality engineering [36]. The Taguchi Method can be used to reduce the number of experiments, obtaining the minimum number of experiments without losing significant information. Taguchi designs are based on orthogonal arrays. These arrays are balanced, ensuring that factor levels can be equally weighted. Therefore, each factor can be studied independently from the other ones [37].

According to the table of parameters that are going to be tested, since the factors have different levels, a mixed level design is required. The appropriate Taguchi design is the L18 design, which presents 18 runs based on one factor with two levels and four factors with three levels: L18(2^1 3^4). Minitab 18 was used to obtain this Taguchi design. The 18 combinations can be seen in Table 4.2.

Experiment Number	Active Length (mm)	Distance Between Electrodes (mm)	Input Voltage (V)	Pulse Repetitions	Pulse Width (µs)
1	10	5	500	40	40
2	10	5	1500	80	70
3	10	5	3000	90	100
4	10	10	500	40	70
5	10	10	1500	80	100
6	10	10	3000	90	40
7	10	20	500	80	40
8	10	20	1500	90	70
9	10	20	3000	40	100
10	15	5	500	90	100
11	15	5	1500	40	40
12	15	5	3000	80	70
13	15	10	500	80	100
14	15	10	1500	90	40
15	15	10	3000	40	70
16	15	20	500	90	70
17	15	20	1500	40	100
18	15	20	3000	80	40

Table 4.2: Table of designed experiments

4.1.2 Experimental Setup

The 18 designed combinations of parameters (Table 4.2) were tested experimentally. A schematic representation of the experimental setup is presented in Figure 4.2. Pictures of the real experimental setups can be seen in Appendix B. The devices and materials that were used are further described.

A transparent cylindrical container made of Polymethyl Methacrylate (PMMA) (40 x 150 mm) was filled with bovine liver tissue. The container was placed in a thermostatic bath at a controlled temperature of 37°C in order to mimic the body core temperature. It was guaranteed that the water level was high enough so that the whole volume of bovine liver tissue placed inside the container would be at that temperature.

Once the water and the bovine liver tissue were uniform at the same temperature of 37°C, a pulse generator system (BTX Gemini X2) was connected to two stainless-steel electrodes inserted in parallel into the liver tissue and delivered a train of pulses, according to the combinations of parameters described in Table 4.2. A high-voltage probe (BTX Enhancer 3000) measured the amplitude of the delivered pulses and displayed the output in a digital oscilloscope.

Fiber optic temperature measurement probes were inserted in the liver tissue to measure the temperature between the two electrodes. For a distance between electrodes of 5 mm, the temperature was measured at the center point between the electrodes. For distances of 10 mm and 20 mm, the temperature was also measured at a second point located 2 mm away from the right electrode, at the same depth of the tip of the electrodes. A thermocouple was inserted in the bovine liver tissue, 3 mm away from the right electrode and also at the same depth of the tip of the electrodes, in order to monitor the temperature outside the electrodes.

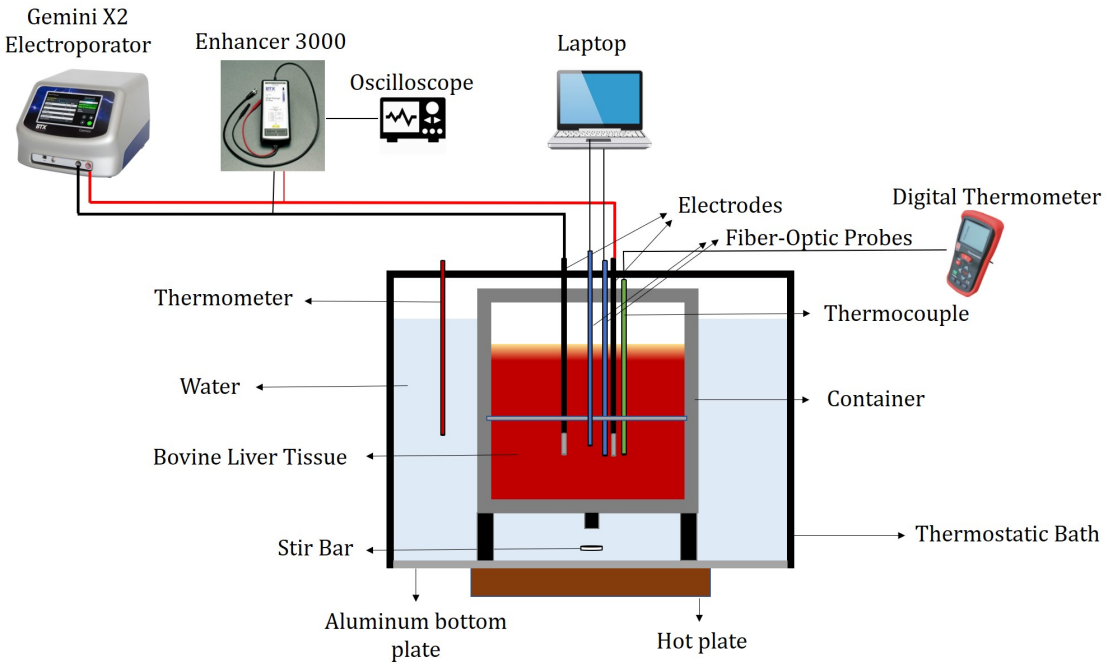

Figure 4.2: 2D scheme of the experimental setup

BTX Gemini X2

The Gemini X2 electroporator is an electroporation system capable of generating pulses to be delivered to the target tissue. The device is capable of generating two different wave pulses: squared or exponential.

For square pulses, the Gemini is capable of delivering up to 99 pulses with maximum intensity of 3000 V. The pulse width can be defined up to 600 µs. The frequency of the pulse delivery can be set between 0.1 Hz and 10 Hz.

The apparatus has a graphical interface that allows the user to define and save the desired protocols. Thus, the pulse parameters were set according to the IRE doses defined to be tested and the device was connected to the pair of electrodes inserted in the bovine liver tissue in order to deliver the pulses.

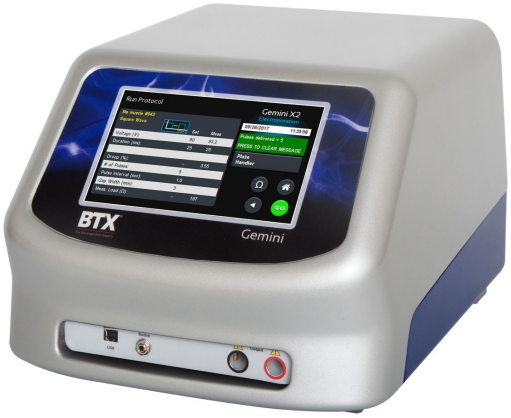

Figure 4.3: BTX Gemini X2 electroporation system

BTX Enhancer 3000 and Digital Oscilloscope

The Enhancer 3000 monitoring system comprehends a High Voltage Probe and an Interface Box. When connected to an oscilloscope or to an other monitoring device it allows a safe monitoring of high voltage signals. The Enhancer 3000 system was therefore connected to a digital oscilloscope (Rohde & Schwarz RTB2004 Oscilloscope) to monitor and record the generated waveforms during the IRE experiments. Moreover, this system provides information about the real amplitude of the pulses that are being delivered to the target tissue.

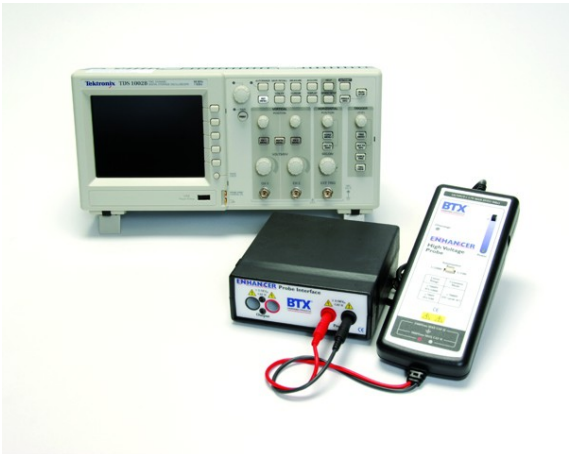

Figure 4.4: Enhancer 3000 monitoring system

Electrodes

The pulses generated by the electroporator were delivered to the bovine liver tissue through a pair of stainless-steel (AISI 302) electrodes with 1 mm diameter. These electrodes were coated with heat shrinking tubing, forming an insulating layer that surrounded the electrodes, except for the part correspondent to the active length.

Hot Plate

The thermostatic bath was placed over a hot plate in order to heat the water to 37°C. The bottom of the bath container was made of aluminum, allowing heat conduction from the hot plate

to the water. The temperature of the hot plate was set at 70°C in order to prevent damage of the plastic containers.

The hot plate system also includes a magnetic stirrer. A stir bar was placed in the bottom of the thermostatic bath in order to allow water circulation on the container and guarantee that the water temperature was uniform.

Neoptix T1 Fiber Optic Temperature Probe

The temperature was measured at two different locations between the electrodes with fiber optic temperature probes. This system is resistant to high electric fields. The probes can measure a wide range of temperature (-270°C to +250°C) with an accuracy of ± 0.2°C. The acquisition rate of the system is 1 sample per second.

The probes are made of PTFE Teflon and their diameter corresponds to Gauge 17 in the Birmingham Gauge system (approximately 1.473 mm).

The measurement principle of this system is based on the temperature dependence of the band gap of gallium arsenide (GaAs). The probes include a GaAs semiconductor crystal at the tip of the fiber which is transparent at wavelengths above 850 nm. The position of the band edge of the GaAs depends on the temperature. When the light is directed via the optical fiber to the crystal, it is absorbed and partially reflected into the fiber. Then, from the position of the band edge, the temperature can be calculated [38].

Thermocouples and Thermometers

A K-type thermocouple (diameter = 1 mm) was used to measure the temperature in the bovine liver tissue, 3 mm away from the right electrode. Internally, the thermocouples contain two wires, one made of Ni Cr^{+}, and the other one made of Ni Al^{-}.
Each thermocouple was connected to a digital thermometer (RS PRO RS41) to display the measured temperature values. Since this device did not provide a data acquisition system, the temperature was monitored by observation.

The accuracy of the measurements can be calculated through Equation 4.1:

$$Accuracy\,(^{\circ}C) = \frac{0.5}{100} \times T + 1 \tag{4.1}$$

being T the temperature displayed by the screen of the thermometer.

Furthermore, an analogue thermometer (Brannan Immersion Glass Thermometer) was used to measure the temperature of the bath and to guarantee that the water would be at a temperature of 37°C.

4.2 Numerical Models

Numerical modeling is a technique that uses mathematical models to describe and simulate physical processes in a system. The system is defined by its geometry and properties of the materials [39].

Two-dimensional models were created in order to analyze the effect of the IRE parameters in the electric field and temperature responses. These 2D models are simpler and faster to compute than 3D models and they can still guarantee a good representation of IRE treatments [25]. The computation of the models was performed using COMSOL Multiphysics v. 5.3, a simulation software for modeling.

The geometry of the models consists of a 2D longitudinal cut perpendicular to the two electrodes, inserted into bovine liver tissue (Figure 4.5). The electrical and thermophysical properties of the bovine liver tissue were found in literature and included into the model.

The Electric Currents and Bioheat Transfer modules of COMSOL were used to define the potential distribution in the media and the heat transfer to the tissue, respectively. Multiphysics were used to couple the effects of both physics. To fully define the model, appropriate boundary conditions were applied. In this case, electrical insulation and thermal insulation of the electrodes were established as the boundary conditions. The liver tissue was also electrically insulated from the external environment. Furthermore, the initial temperature of the tissue was set at 37°C in order to simulate the physiological temperature of the human body.

Figure 4.5: Physical geometry of the simulation models

4.2.1 Finite Element Method

The equations involved in the mathematical models are often partial differential equations, which are usually difficult to solve. Finite Element Method (FEM) can be used to approximate the solutions of these equations. It divides the geometry domain into smaller parts creating a mesh of elements [40]. These elements are then modeled by simple differential equations related to the phenomena in study.

If the mesh is too coarse, it may lead to undesirable errors when solving the model. On the other hand, if the mesh is too fine, the simulation might require a long computation time, depending on the capability of the computer that is used to run the simulation. As a result, there should be a compromise between computation time and resolution. Usually, one would prefer to choose a better mesh resolution in the regions of interest. In addition, the borders between regions with different material properties may also be a problem and they should have higher mesh resolution [40].

The mesh was built using the physics-controlled mesh option of COMSOL. The resolution was defined as "extremely fine". The elements had a triangular shape. A graphical example of a mesh is presented in Figure 4.6. According to the tested values of active length and distance between electrodes, the created mesh changed slightly in the number of elements. The number of elements for each configuration of electrodes is presented in Table 4.3.

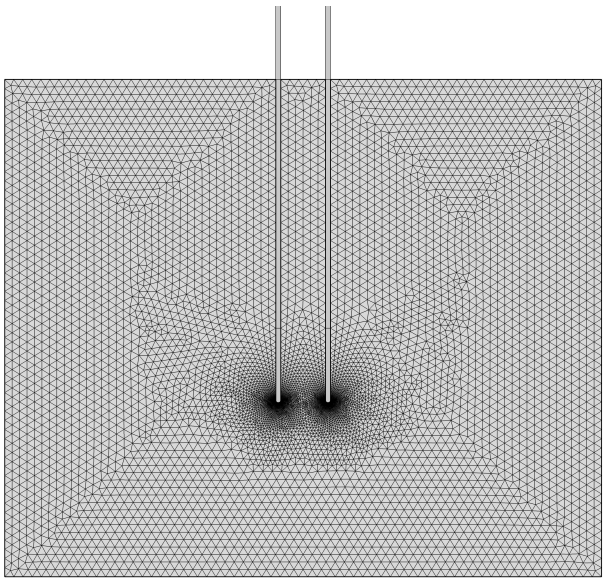

Figure 4.6: Finite Element Method (Distance between electrodes: 10 mm; Active length: 15 mm)

Distance Between Electrodes (mm)	Active Length (mm)	Number of Elements
5	10	14605
5	15	14641
10	10	15276
10	15	15468
20	10	15876
20	15	15980

Table 4.3: Number of elements for each electrode configuration

4.2.2 Mathematical Models

Electric Currents

The electric field distribution in the tissue is represented by the Laplace equation:

$$\nabla^2 \cdot V = 0 \tag{4.2}$$

The Laplace equation can also be represented in 2D cartesian coordinates by:

$$\frac{\partial^2 V}{\partial x^2} + \frac{\partial^2 V}{\partial y^2} = 0 \tag{4.3}$$

Equation 4.4, Equation 4.5 and Equation 4.7 represent the current conservation in the tissue.

$$\nabla \cdot J = Q_{j,v} \tag{4.4}$$

being J the current density (A/m^2) and $Q_{j,v}$ the distributed current source, which is null in this situation.

The second equation is depicted by Equation 4.5:

$$J = \sigma E + \frac{\partial D}{\partial t} + J_e \tag{4.5}$$

where σ is the electrical conductivity of the material, E is the electric field intensity and J_e is the external current density. $\frac{\partial D}{\partial t}$ is the displacement current in which D is the electric displacement field and it is related to time-varying electric fields. The constitutive relation is displayed in Equation 4.6. It describes the macroscopic properties of the medium, relating the electric displacement D with the electric field E. ε_r is the relative permittivity of the medium and ε_0 the permittivity of free space.

$$D = \varepsilon_0 \varepsilon_r E \tag{4.6}$$

Equation 4.7 expresses the electric field as the gradient of voltage, representing that the electric field E points from regions of high electric potential to regions of low electric potential.

$$E = -\nabla V \tag{4.7}$$

Electric insulation was applied as a boundary condition to the electrodes, except for the exposed tips. The tissue was also assumed as electrically insulated from the surrounding environment. This means that no electric current flows through the boundary, being the electric potential discontinuous across the same:

$$n \cdot J = 0 \tag{4.8}$$

Bioheat Transfer

The Bioheat Transfer Equation, also referred to as the Pennes' Bioheat Equation [41], is represented in Equation 4.9. To model heat transfer within biological tissue it is necessary to take into account the metabolic heat generation and the exchange of thermal energy between blood flow and the biological tissue. As such, Pennes modified the general heat conduction equation by introducing a term that take these phenomena into account [42].

$$\rho c_p \frac{\partial T}{\partial t} + \rho c_p u \cdot \nabla T + \nabla \cdot q = Q_s + Q_{bio} \tag{4.9}$$

The first term of the equation represents temperature changes in time whereas the second term represents the effect of a moving coordinate system, which is required to model, for instance, a translational motion of a heat source. Q_s is the energy source term, sometimes mentioned as specific absorption rate (SAR) in the literature [23]. Q_{bio} can be referred as the bioheat term.

Equation 4.10 displays the Fourier's Law of Heat Conduction, which represents the energy transport due to thermal diffusion within the tissue.

$$q = -k \nabla T \tag{4.10}$$

being k the thermal conductivity of the tissue and ∇T the temperature gradient.

The bioheat term Q_{bio}, present in the Bioheat Transfer Equation, is mathematically described in Equation 4.11. It contains the perfusion source term Q_{bl} and the metabolic heat generation term Q_{met}, representing the phenomena of heat transfer in biological tissue.

$$Q_{bio} = Q_{bl} + Q_{met} \tag{4.11}$$

The perfusion source term Q_{bl} is presented in Equation 4.12. It describes the energy added or removed due to the convective blood flow into and out of the tissue.

$$Q_{bl} = \rho_b \, c_{p,b} \, \omega_b \, (T_b - T) \tag{4.12}$$

where ρ_b is the blood density, T_b the arterial blood temperature and T represents the temperature in the tissue. The specific heat of blood $c_{p,b}$ describes the amount of heat required to produce a unit temperature change in a unit mass of blood. The blood perfusion rate ω_b describes the volume of blood per second that flows through a unit volume of tissue.

The metabolic heat source Q_{met} represents the heat generation from metabolism. In this case, this term can be disregarded since its effect in the presence of applied heat generation is usually negligible [43].

Thermal insulation was applied to the model as a boundary condition. Therefore, there is no heat flux across the boundary, this is, the temperature gradient across the boundary is zero:

$$-n \cdot q = 0 \tag{4.13}$$

4.2.3 Electrical and Thermophysical Properties

The electrical and thermophysical properties used in the models are summarized in this section. Table 4.4 presents the terms used to represent blood perfusion and metabolism to model heat transfer in biological tissue.

Parameter	Symbol	Unit	Value	Reference
Blood Density	ρ_b	Kg/m^3	1000	[23]
Blood Temperature	T_b	°C	37	-
Blood Specific Heat Capacity	$c_{p,b}$	J/(Kg·°C)	3640	[23]
Blood Perfusion Rate	ω_b	1/s	5e^{-4}	[23]
Metabolic Heat Source	Q_{met}	W/m^3	0	[43]

Table 4.4: Bioheat properties

The electrical and thermophysical properties of bovine liver tissue are presented in Table 4.5. The heat capacity $c_{p,bov}$ and thermal conductivity k_{bov} were set according to their changes with temperature, whose values are plotted in Figure 4.7 and Figure 4.8, respectively.

Parameter	Symbol	Unit	Value	Reference
Density	ρ_{bov}	Kg/m^3	1050	[44]
Electrical Conductivity	σ_{bov}	S/m	0.333	[45]
Heat Capacity	$c_{p,bov}$	J/(Kg·°C)	see Figure 4.7	[46]
Relative Permittivity	$\epsilon_{r,bov}$	-	53	[46]
Thermal Conductivity	k_{bov}	W/(m·°C)	see Figure 4.8	[47]

Table 4.5: Electrical and thermophysical properties of bovine liver tissue

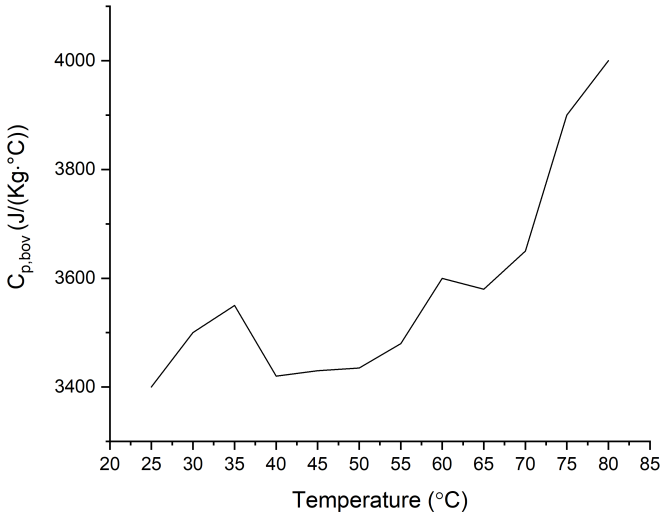

Figure 4.7: Heat capacity of bovine liver tissue [46]

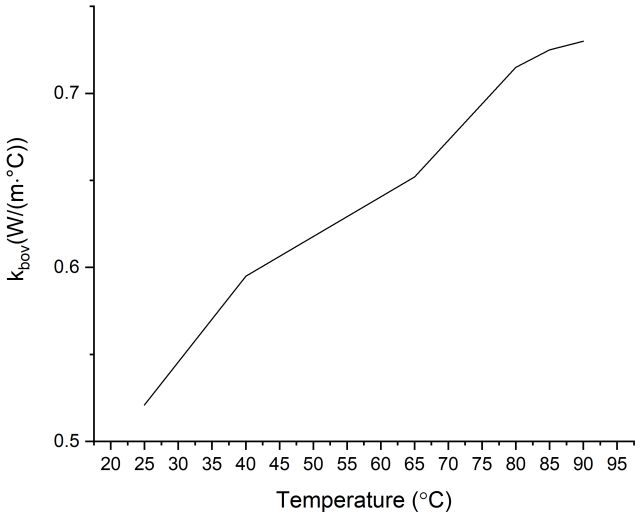

Figure 4.8: Thermal conductivity of bovine liver tissue [47]

5 Experimental Validation of the Simulation Models

The results of the IRE experiments performed in bovine liver tissue are presented in this chapter. The 18 combinations of parameters presented in Table 4.2 were considered for the experiments. All the experiments were done successfully except for experiments 3 and 12. It was not possible to obtain data from these two experiments due to the high currents produced during these experiments. The Gemini X2 electroporator stopped both experiments automatically for safety reasons.

Two trials of experiments were performed. The temperature changes obtained from the experiments were then compared to the ones obtained from the simulation models in order to validate them for biological tissue. Statistical analysis was performed to evaluate the influence of the tested parameters in the maximum temperature achieved in the tissue.

5.1 Analysis of the Pulse Trains

The generation and delivery of the pulses to the tissue presented some discrepancies relatively to the designed parameters in Table 4.2. As a result, experimental measurements of the amplitude and duration of the delivered pulses were made to assess the real values that were being applied during the experiments. These real values of applied voltage and pulse width were inserted in the simulation models instead of the set values in order to match the experimental settings and the models. Furthermore, it improves the accuracy of the results obtained from the models because it is a more reliable representation of the real phenomena.

5.1.1 Experimental Applied Voltage

The applied voltage was measured in each experiment using the Enhancer 3000 system. The high-voltage probe was connected to the digital oscilloscope to record the signal of the train of applied pulses. For the experiments with 40 pulses, the acquisition rate of the oscilloscope was 333 kSamples/s (1 data point each 3 μs). For the experiments with 80 or 90 pulses, the acquisition rate was 167 kSamples/s (1 data point each 6 μs).

The pulse train signal contains information about the amplitude of each delivered pulse. The maximum value of voltage measured in each pulse was assumed as the amplitude of the pulse. In the end, the applied voltage of each experiment was calculated as the average of the amplitudes of all the delivered pulses during that experiment. The applied voltages for each experiment in both trials are presented in Table 5.1.

Experiment Number	Applied Voltage (V)		
	Set Voltage	Experiment (Trial 1)	Experiment (Trial 2)
1	500	522	532
2	1500	1556	1547
3	3000	-	-
4	500	523	530
5	1500	1551	1551
6	3000	3053	3039
7	500	519	521
8	1500	1556	1550
9	3000	3079	3063
10	500	525	530
11	1500	1555	1553
12	3000	-	-
13	500	522	528
14	1500	1549	1556
15	3000	3063	3056
16	500	523	526
17	1500	1558	1564
18	3000	3048	3058

Table 5.1: Voltage applied in each experiment

5.1.2 Experimental Pulse Width

The duration of each delivered pulse was measured by the Gemini X2 electroporator. The range of pulse widths was measured for each experiment. The maximum value in that range was considered the pulse width of the experiment. The values are presented in Table 5.2.

Experiment Number	Pulse Width (μs)		
	Set Width	Experiment (Trial 1)	Experiment (Trial 2)
1	40	40	40
2	70	75	74
3	100	-	-
4	70	70	70
5	100	106	106
6	40	44	44
7	40	40	40
8	70	76	76
9	100	106	105
10	100	100	100
11	40	44	43
12	70	-	-
13	100	100	100
14	40	44	43
15	70	74	73
16	70	70	70
17	100	106	106
18	40	44	44

Table 5.2: Experimental pulse width of each experiment

5.2 Temperature Measurements

5.2.1 Calibration of the Temperature Probes

The fiber-optic probes and the thermocouple were calibrated to assure that the temperature readings were accurate and reliable. The probes were inserted in a water container. The temperature of the water was varied between 20°C and 95°C according to the value displayed by a reference thermometer. Temperature measurements were made every 5°C with the three probes. In the end, an interpolation curve was calculated for each probe. When analysing the data, the temperature values obtained from the probes were introduced in the calibration curves to obtain more accurate measurements.

5.2.2 Comparison Between Experimental and Simulation Results

Temperature was measured at three different points in the bovine liver tissue, experimentally and by simulation. Two measurements were made in the area between the electrodes, at the center point and 2mm from the electrode (except for the cases where the distance between electrodes was 5 mm, where it was only possible to make experiments at the center point between the electrodes). Another measurement was made 3 mm away from the right electrode to monitor the temperature outside the target area.

The experimental measurements were used to validate the simulation models. If the temperature values measured experimentally by the probes are similar to the values calculated from the simulation models, then the model can be assumed as a reliable representation of the real phenomena. In other words, if the error between the temperature measured experimentally and the temperature calculated by simulation is low, then the model can be validated. As a result, the percentage error between experiments and simulation models was calculated for each one of the three measurement points. The experimental results were taken as the ground truth. The formula that was used to calculate the errors is presented in Equation 5.1:

$$Error\,(\%) = \frac{|T_{model} - T_{experiment}|}{T_{experiment}} \times 100 \tag{5.1}$$

The percentage error at the two locations between the electrodes was calculated for each data sample acquired from the fiber-optic probes (1 temperature measure per second). In the end, the percentage error of each experiment was taken as the average of the errors calculated in every second of the experiment. For the thermocouple, only the measurement taken at the last second of the experiment was considered. Therefore, the percentage error was calculated only at that moment.

It was assumed that a percentage error less or equal to 10% would be acceptable for model validation. Furthermore, it was given more emphasis to the measurements that were made between the electrodes since that is the area of interest where electric fields are generated. Therefore, it is also expected a higher increase of temperature in this area than outside the electrodes.

5.3 Validation of the Models

Error plots are presented in three different graphs, according to each distance between electrodes. A graph with the maximum temperature measured by each probe and the corresponding temperature calculated by the models at the same locations is also provided. The accuracies of the measuring instruments were also included in the temperature graphs as error bars.

5.3.1 Distance Between Electrodes: 5 mm

The combinations of parameters with a distance between electrodes of 5 mm tested in both trials are presented in Table 5.3 and Table 5.4. It was only possible to present results from 4 of the 6 planned experiments with a 5 mm distance between electrodes. In both experiments 3 and 12, the applied voltage of 3000 V would result in a high voltage-to-distance ratio of 6000 V/cm. The current during the pulse delivery was too high and the Gemini stopped the experiment immediately for safety reasons.

The maximum temperature measured at the center point between the electrodes and 3 mm away from one of the electrodes is presented for each experiment in Figure 5.1. Figure 5.2 presents the percentage errors for each experiment.

Distance Between Electrodes: 5 mm				
Experiment Number	**Active Length (mm)**	**Input Voltage (V)**	**Pulse Repetitions**	**Pulse Width (µs)**
1	10	522	40	40
2	10	1556	80	75
10	15	525	90	100
11	15	1555	40	44

Table 5.3: Table of experiments with a distance between electrodes of 5 mm (Trial 1)

Distance Between Electrodes: 5 mm				
Experiment Number	**Active Length (mm)**	**Input Voltage (V)**	**Pulse Repetitions**	**Pulse Width (µs)**
1	10	532	40	40
2	10	1547	80	74
10	15	530	90	100
11	15	1553	40	43

Table 5.4: Table of experiments with a distance between electrodes of 5 mm (Trial 2)

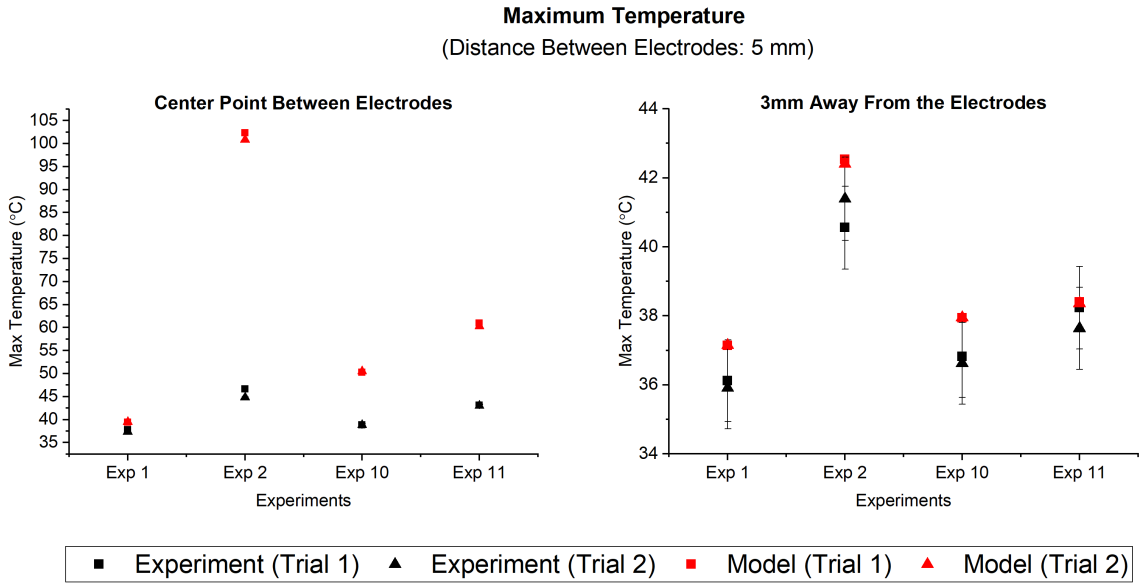

Figure 5.1: Maximum temperature for each experiment with a distance between electrodes of 5 mm

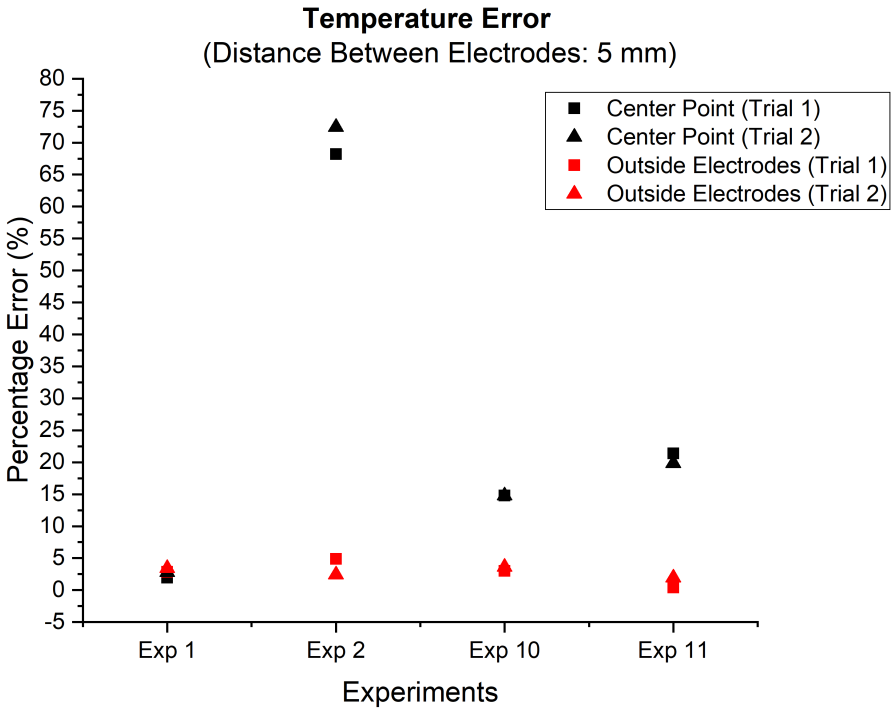

Figure 5.2: Percentage error for each experiment with a distance between electrodes of 5 mm

Relatively high percentage errors were found between experiments and simulations for a separation between electrodes of 5 mm.

From Figure 5.2 it is possible to see that only experiment 1 revealed low percentage errors. The applied voltage in this experiment results in a slight increase of the temperature, as it is possible

to see from the maximum temperatures presented in Figure 5.1. Therefore, the error between experimental and simulation measurements achieved in this experiment was not significant.

For the other three experiments that were performed, although the errors regarding the measurements outside the electrodes were relatively small, the errors of the temperature measurement in the region where the electric field is generated were too high to be acceptable.

Summing up, only one out of four experiments performed with a 5 mm distance between electrodes presented low errors between experimental and simulation results. Consequently, the model cannot be validated for this distance. It does not allow for a good representation of reality when the electrodes are separated by a distance of 5 mm.

5.3.2 Distance Between Electrodes: 10 mm

The combinations of parameters tested for a distance between electrodes of 10 mm are presented in Table 5.5 and Table 5.6 for trials 1 and 2, respectively.

The maximum temperatures measured at the three locations are shown in Figure 5.3. Figure 5.4 presents the percentage errors obtained in each experiment.

Distance Between Electrodes: 10 mm				
Experiment Number	**Active Length (mm)**	**Input Voltage (V)**	**Pulse Repetitions**	**Pulse Width (µs)**
4	10	523	40	70
5	10	1551	80	106
6	10	3053	90	44
13	15	522	80	100
14	15	1549	90	44
15	15	3063	40	74

Table 5.5: Table of experiments with a distance between electrodes of 10 mm (Trial 1)

Distance Between Electrodes: 10 mm				
Experiment Number	**Active Length (mm)**	**Input Voltage (V)**	**Pulse Repetitions**	**Pulse Width (µs)**
4	10	530	40	70
5	10	1551	80	106
6	10	3039	90	44
13	15	528	80	100
14	15	1556	90	43
15	15	3056	40	73

Table 5.6: Table of experiments with a distance between electrodes of 10 mm (Trial 2)

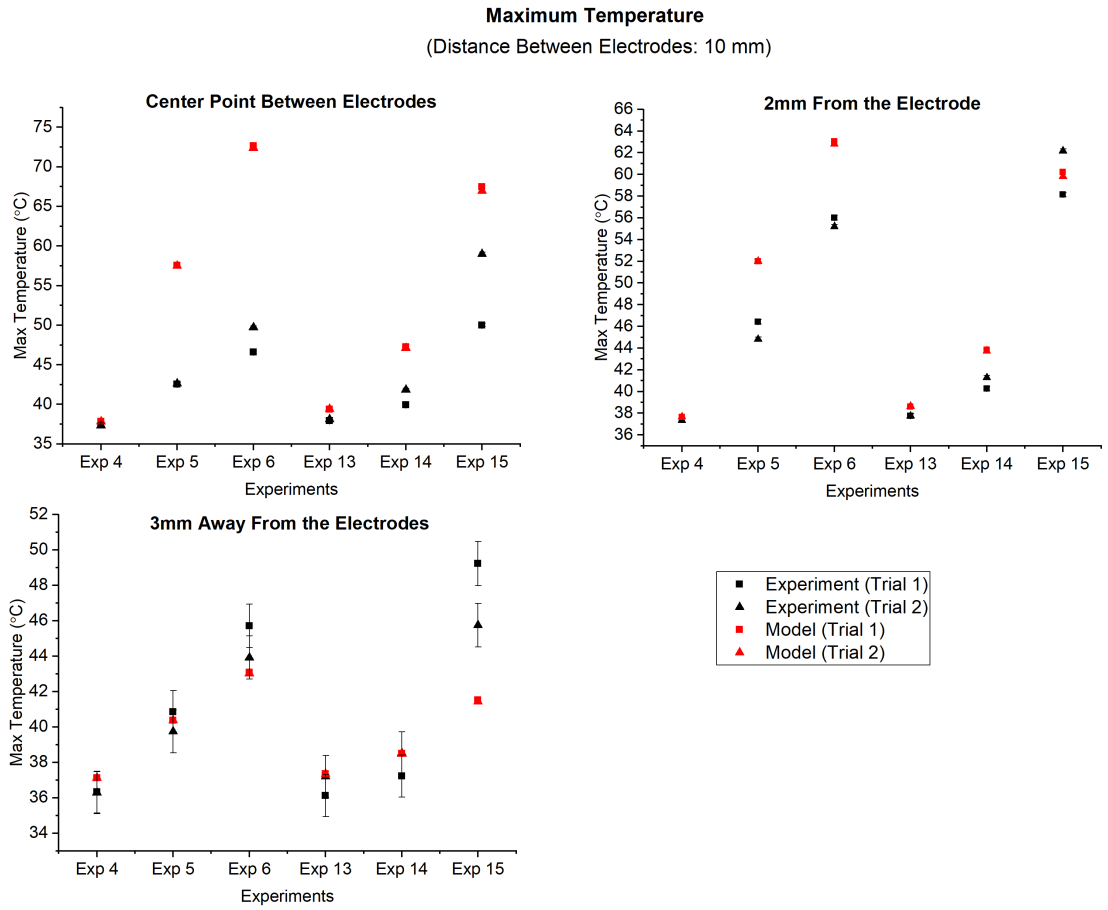

Figure 5.3: Maximum temperature for each experiment with a distance between electrodes of 10 mm

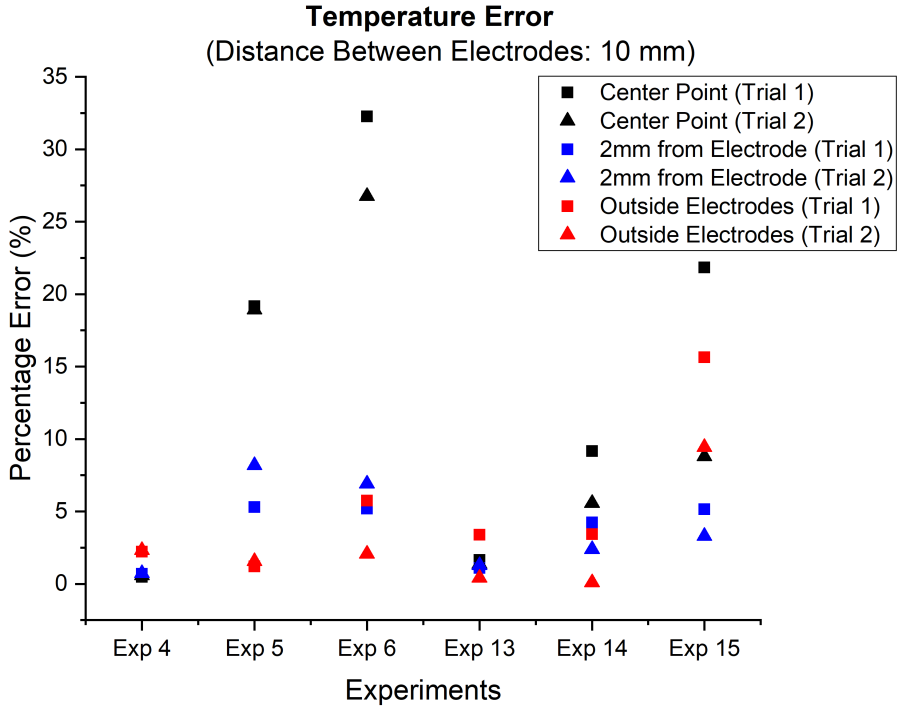

Figure 5.4: Percentage error for each experiment with a distance between electrodes of 10 mm

With a 10 mm distance between electrodes, and although there were some cases that revealed unacceptable high errors, the percentage errors seemed to be, in general, lower than the ones found for a shorter distance of 5 mm.

Experiments 4 and 13 achieved low errors as it is shown in Figure 5.4. The voltage applied during these experiments was low and therefore the temperature was not expected to increase substantially, as it is displayed in Figure 5.3. Experiment 14 also obtained acceptable errors under 10% for all the measurements.

On the other hand, experiments 5 and 6 obtained high error percentages on the measurements made at the center point between the electrodes. In experiment 15, although the error obtained in the first trial was high, the measurement done in the second trial was more acceptable, presenting an error around 10%. Furthermore, the errors obtained in the measurements made at the other location point between the electrodes were acceptable in all experiments.

Considering all this, the model can be validated for a separation of electrodes of 10 mm.

5.3.3 Distance Between Electrodes: 20 mm

Table 5.7 and Table 5.8 display the combinations of parameters that were tested for a distance between electrodes of 20 mm.

The maximum temperatures measured between and outside the electrodes are shown in Figure 5.5. Figure 5.6 shows the errors between experiment and simulation obtained in each experiment.

Distance Between Electrodes: 20 mm				
Experiment Number	**Active Length (mm)**	**Input Voltage (V)**	**Pulse Repetitions**	**Pulse Width (µs)**
7	10	519	80	40
8	10	1556	90	76
9	10	3079	40	106
16	15	523	90	70
17	15	1558	40	106
18	15	3048	80	44

Table 5.7: Table of experiments with a distance between electrodes of 20 mm (Trial 1)

Distance Between Electrodes: 20 mm				
Experiment Number	**Active Length (mm)**	**Input Voltage (V)**	**Pulse Repetitions**	**Pulse Width (µs)**
7	10	521	80	40
8	10	1550	90	76
9	10	3063	40	105
16	15	526	90	70
17	15	1564	40	106
18	15	3058	80	44

Table 5.8: Table of experiments with a distance between electrodes of 20 mm (Trial 2)

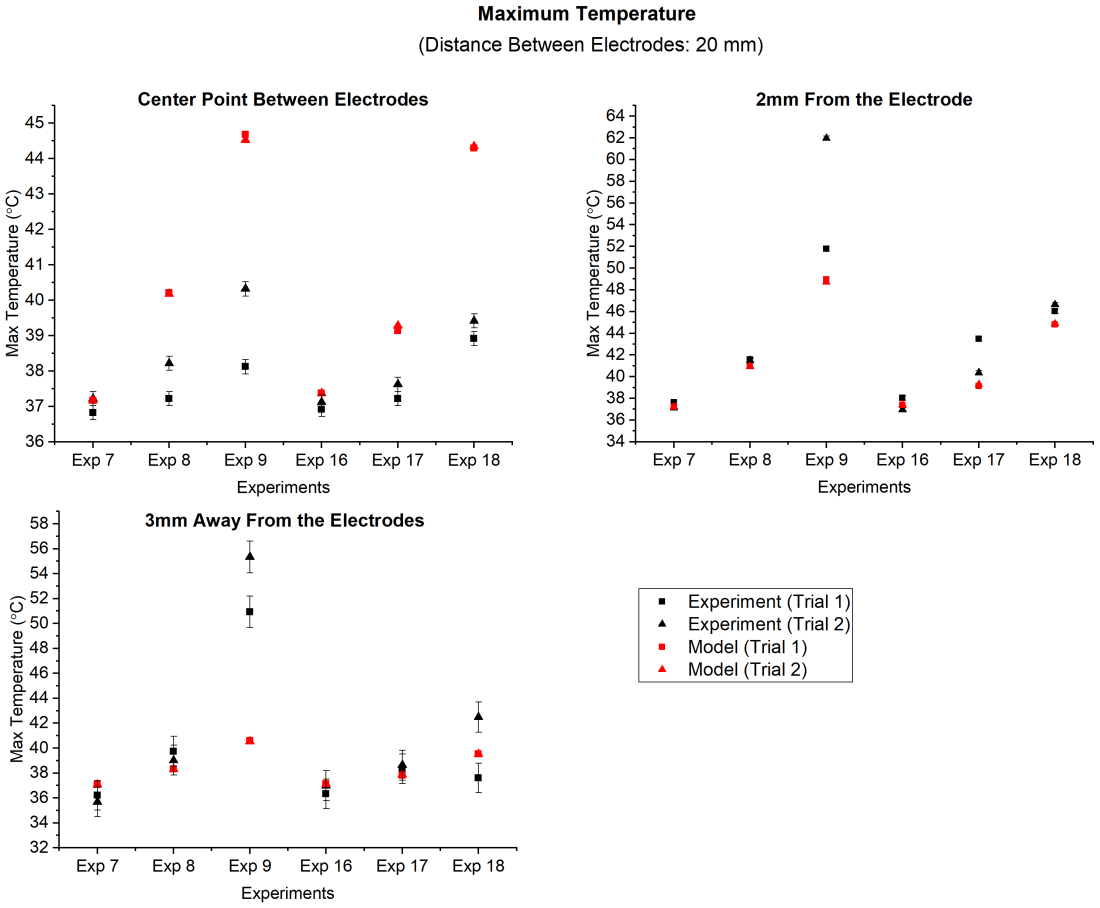

Figure 5.5: Maximum temperature for each experiment with a distance between electrodes of 20 mm

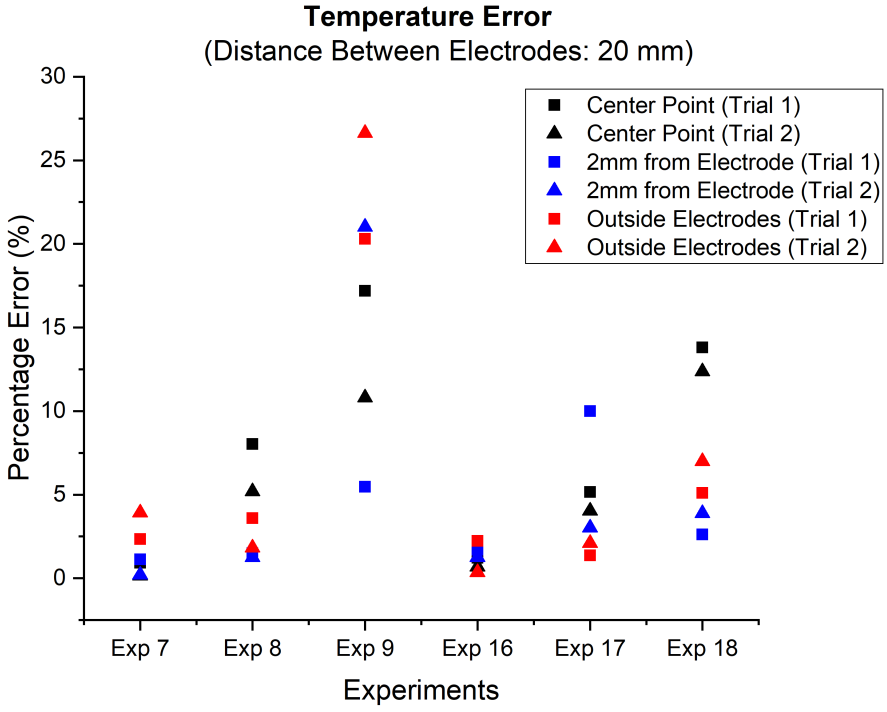

Figure 5.6: Percentage error for each experiment with a distance between electrodes of 20 mm

The obtained errors for this configuration of electrodes were, in general, lower than for the other shorter distances between the electrodes that were tested.

Experiments 7, 8 and 16 presented errors below 10% for all measurements. On the other hand, experiment 9 presented higher error values in general, compared to the other experiments. Still, the measurement made at the point closer to the electrode in the first trial of measurements was acceptable.

In experiments 9 and 18, some measurements of the temperature at the center point exceeded the 10% limit. On the other hand, there were acceptable measurements at 2 mm from the electrode in both experiments, as well as the values obtained at the point outside the electrodes.

This way, it is possible to affirm that the model can be validated for configurations with a distance between electrodes of 20 mm.

5.4 Statistical Analysis: ANOVA

The analysis of the temperature outcomes allowed to validate the model for distances between electrodes in the range of 10 to 20 mm.

Once validated, a statistical analysis of the temperature results obtained from the models was performed to investigate the influence of each studied parameter in the maximum temperature achieved in the tissue.

An analysis of variance (ANOVA) was performed using IBM SPSS Statistics 24. The maximum temperatures in the bovine liver tissue obtained from the simulation models were considered, taking into account the combinations of parameters of the previously designed experiments. Only the experiments corresponding to the validated models were considered. Therefore, combinations 1 to 3 and 10 to 12 (Table 4.2) were not included in this analysis. Results with a p-value lower than 0.05 ($p < 0.05$) were considered as statistically significant. However, no significant parameters were found using the results obtained from these combinations of parameters. The p-values of each parameter can be found in Table 5.10.

As a result, in order to obtain significance, the sample size was increased by measuring the maximum temperature after applying 40, 60, 80 and 90 pulses for the 12 combinations of parameters that were previously considered. Table 5.9 presents the maximum temperatures achieved for the 48 situations.

Experiment Number	Maximum Temperature (°C)			
	At 40 Pulses	At 60 Pulses	At 80 Pulses	At 90 Pulses
4	37.873	38.153	38.471	38.622
5	48.185	51.83	55.877	57.755
6	54.778	60.523	66.782	69.686
7	37.215	37.267	37.314	37.336
8	40.371	41.183	41.931	42.272
9	55.979	60.467	64.486	66.307
13	38.236	38.658	39.177	39.428
14	41.453	43.021	44.892	45.795
15	67.316	77.297	88.591	94.007
16	37.366	37.456	37.538	37.575
17	41.688	42.826	43.882	44.366
18	44.486	46.301	47.976	48.743

Table 5.9: Maximum temperature after the delivery of 40, 60, 80 and 90 pulses (obtained from simulation)

The distance between electrodes, the applied voltage and pulse width were found to have significant influence on the maximum temperature. On the other hand, the pulse repetitions and the active length did not seem to have a significant impact on the maximum temperature. The p-values for each parameter are summarized in Table 5.10.

Parameter	p-value with 12 combinations	p-value with 48 combinations
Active Length	0.481	0.788
Applied Voltage	0.057	< 0.001
Distance Between Electrodes	0.117	< 0.001
Pulse Repetitions	0.824	0.107
Pulse Width	0.827	0.002

Table 5.10: p-values of the ANOVA test for each IRE parameter

6 IRE Optimization for the Treatment of Pancreatic Cancer

After validating the simulation models for biological tissue, the IRE parameters can be optimized for the treatment of pancreatic cancer.

As a result, the properties of human pancreatic tissue were introduced in the models. Calculations of the electric field between the electrodes and maximum surface temperature were made for the designed experiments that were in the validation range. Using these results, the optimal IRE dose for pancreatic cancer was estimated using Response Surface Methodology.

The optimal IRE dose was then included in the models and the electric field and temperature distributions were simulated.

6.1 Properties of Pancreatic Tissue

Assuming that the simulation models were validated for biological tissue, the electrical and thermophysical properties of the human pancreas were introduced in the model. These properties are described in Table 6.1.

Parameter	Symbol	Unit	Value	Reference
Density	ρ	Kg/m^3	1080	[48]
Electrical Conductivity	σ	S/m	0.145	[49]
Heat Capacity	C_p	J/(Kg·°C)	3164	[49]
Relative Permittivity	ϵ_r	-	3200	[50]
Thermal Conductivity	k	W/(m·°C)	0.52	[49]

Table 6.1: Electrical and thermophysical properties of human pancreatic tissue

The electric field at the center point between the electrodes and the maximum temperature achieved in the tissue were calculated for each of the 12 designed experiments that were in the validation range. The results are presented in Table 6.2.

Experiment	Electric Field (V/cm)	Maximum Temperature (°C)
4	541.94	37.413
5	1625.8	42.286
6	3251.7	52.625
7	226.33	37.149
8	679	39.513
9	1358	46.199
13	553.18	38.012
14	1659.5	41.058
15	3319.1	51.753
16	246.18	37.273
17	738.55	39.235
18	1477.1	42.261

Table 6.2: Electric field and maximum temperature results of the validated experiments in pancreatic tissue

6.2 Response Surface Methodology

In modeling, Response Surface Methodology (RSM) is usually applied for the enhancement of the response variables, exploring the relation between these responses and the explanatory variables [51].

RSM was performed to obtain the optimal IRE dose. The optimization approach consisted in maximizing the electric field generated between the electrodes during the IRE procedure without achieving thermal damage in the tissue. Thermal damage was assumed to occur at temperatures higher than 50°C. For this reason, a target temperature of 50°C was set.

A central composite design was used for the optimization. Data from the 12 validated experiments were considered for the estimation of the optimal response. The five continuous factors in study were included: active length, distance between electrodes, pulse repetitions, pulse width and voltage. Although it was previously verified by the ANOVA test that some factors did not have statistical significance on the maximum temperature, all of them were included in the RSM in order to obtain the optimal IRE Dose. Two continuous responses were optimized: the maximum temperature and the electric field.

RSM was performed using Minitab 18. The optimization plot is presented in Figure 6.1.

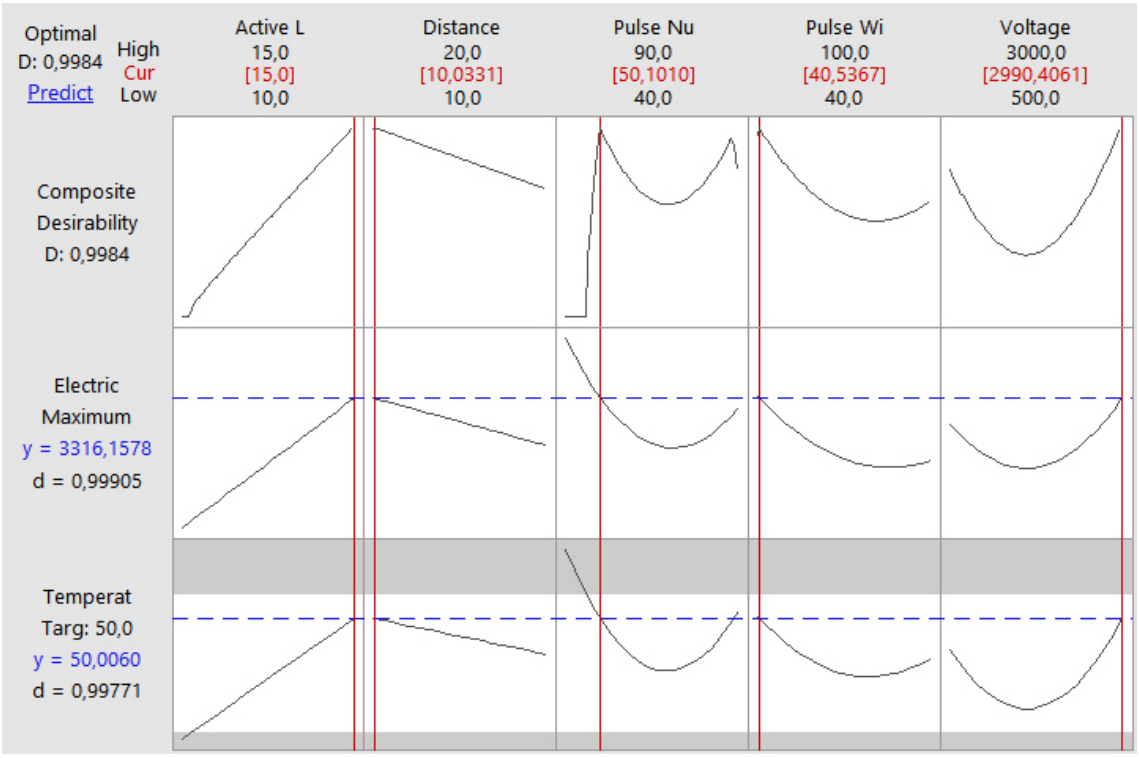

Figure 6.1: Optimization results obtained from RSM

The optimal parameters are presented on the top row, between brackets and in red. The red lines in the graph represent the optimal solutions. The blue dashed lines represent the target values of the objective functions, in this case, the maximum electric field and a temperature of 50°C. The gray areas indicate that the response has zero desirability in that zone.

The individual desirability (d) evaluates how well the settings optimize a single response. RSM calculates d through Equation 6.1 to maximize the electric field and through Equation 6.2 to target the maximum temperature [52].

$$d_i = \begin{cases} 0, \widehat{y}_i < L_i \\ (\frac{\widehat{y}_i - L_i}{T_i - Li})^{r_i}, L_i \leq \widehat{y}_i \leq T_i \\ 1, \widehat{y}_i < T_i \end{cases} \tag{6.1}$$

$$d_i = \begin{cases} (\frac{\widehat{y}_i - L_i}{T_i - Li})^{r_i}, L_i \leq \widehat{y}_i \leq T_i \\ (\frac{U_i - \widehat{y}_i}{U_i - Ti})^{r_i}, T_i \leq \widehat{y}_i \leq U_i \\ 0, \widehat{y}_i < L_i \\ 0, \widehat{y}_i > U_i \end{cases} \tag{6.2}$$

being d_i the desirability for the ith response, $\widehat{y}_i$ the predicted value of the ith response, L_i the lowest acceptable value for the ith response, T_i the target value of the ith response, and r_i the weight of the desirability function of the ith response.

The composite desirability (D) does an overall evaluation of how well the combination of variables optimizes the defined set of responses, representing the closeness of a response to its ideal value. The optimal solution occurs when composite desirability is at its maximum value ($D = 1$). RSM calculated D using Equation 6.3 [53] :

$$D = (d_1 \times d_2)^{\frac{1}{2}} \tag{6.3}$$

being d_1 and d_2 the individual desirabilities of the electric field and maximum temperature.

The individual desirability for the electric field response ($d = 0.99905$) was close to the maximum value of 1, which means that this response was well optimized. Same way, the maximum temperature also achieved a high individual desirability ($d = 0.99771$) meaning that it was also well optimized.

A composite desirability of $D = 0.9984$ was obtained, meaning that the settings seem to achieve good results for all responses as a whole.

The optimal parameters are summarized in Table 6.3. The number of pulse repetitions was defined as 50 instead of the result of 50.1010 calculated by RSM.

Parameter	**Optimal Value**
Active Length	15 mm
Distance Between Electrodes	10.0331 mm
Pulse Repetitions	50 Pulses
Pulse Width	40.5367 µs
Applied Voltage	2990.4061 V

Table 6.3: Optimal IRE Dose for pancreatic cancer

6.3 Analysis of the RSM Results

The optimal parameters obtained from RSM were inserted in the simulation models to assess the reliability of the method. The electric field was calculated at the center point between the electrodes. The maximum temperature achieved on the surface was also measured. The outcomes of each response were compared with the ones obtained with RSM. By calculating the percentage error between both measurements it was assessed if the optimization process made by RSM was reliable. The errors for the electric field and for the maximum temperature were calculated using Equation 6.4 and Equation 6.5, respectively. The measurements of electric field and temperature obtained from the simulation models were assumed as the ground truth.

$$Error\,(\%) = \frac{|E_{RSM} - E_{model}|}{E_{model}} \times 100 \tag{6.4}$$

$$Error\,(\%) = \frac{|T_{RSM} - T_{model}|}{T_{model}} \times 100 \tag{6.5}$$

There was a good agreement between the electric field calculated by RSM and by the simulation model. The error on the maximum temperature was larger than the one of the electric field. However, RSM made an overestimation of the temperature. The maximum temperature obtained from simulation was 46.796°C, which is less than the threshold for thermal damage (50°C). Therefore, the error is not significant, since it is less likely that thermal damage occurs in the tissue.

Table 6.4 compares the electric field and temperature results obtained with RSM and with the simulation models.

Response	RSM	Simulation Model	Error
Electric Field (V/cm)	3316.1578	3296.1	0.61%
Maximum Temperature (°C)	50.0060	46.796	6.86%

Table 6.4: Comparison of the optimization and simulation results with the optimal IRE dose for pancreatic cancer

6.4 Electric Field and Temperature Distributions for the Optimal IRE Dose

Once verified the reliability of the optimization process, the electric field and temperature distributions on pancreatic tissue were calculated also by simulation. The physics-controlled option of COMSOL was used to build the FEM mesh. The resolution was set as "extremely fine". The mesh consisted of 15482 triangular elements.

The graphical representation of the electric field and temperature distributions in the pancreatic tissue are displayed in Figure 6.2 and Figure 6.3, respectively.

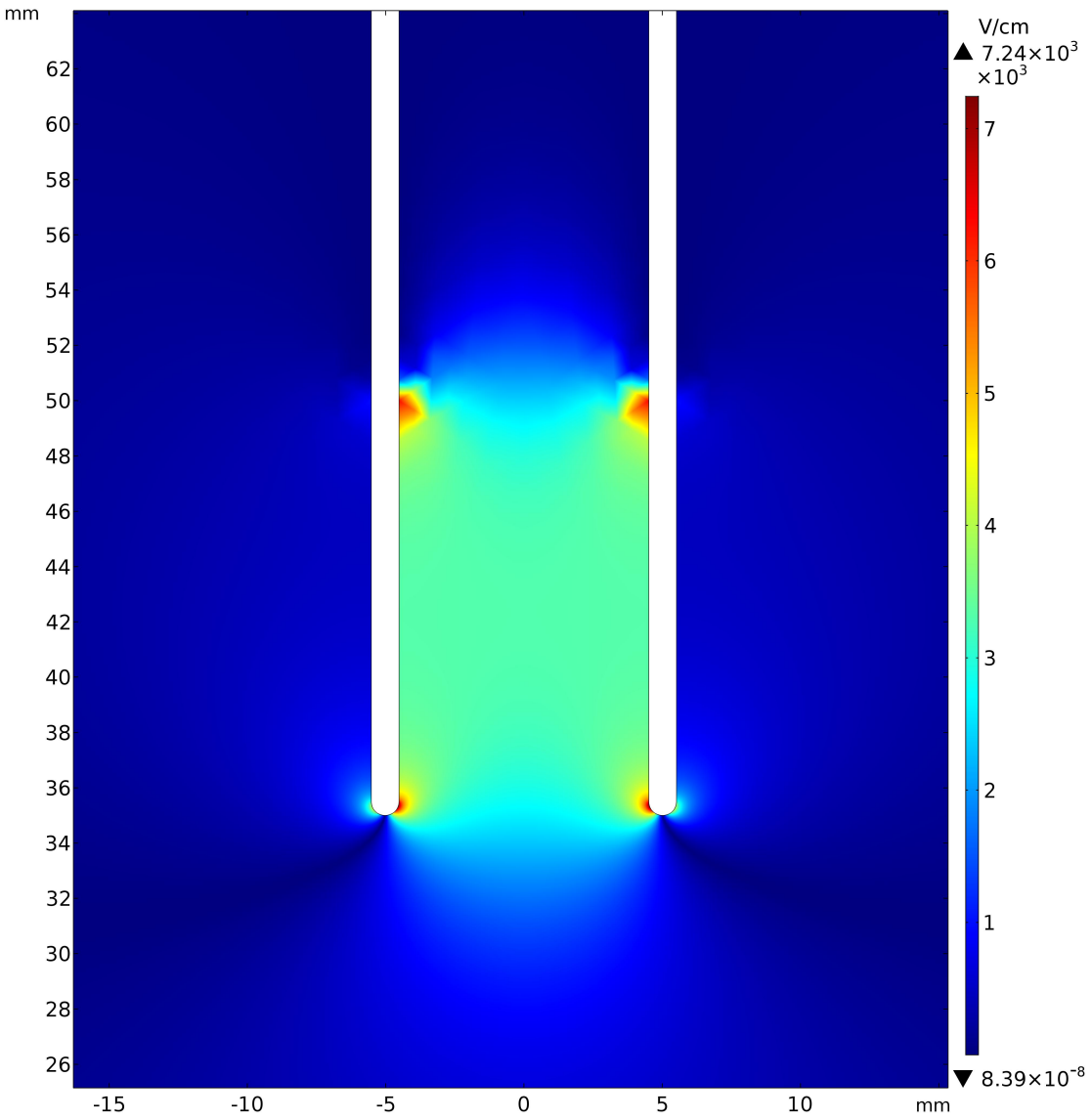

Figure 6.2: Electric field distribution in pancreatic tissue when applying the optimal IRE dose

An approximated value for the generated electric field between the electrodes can be estimated by the voltage-to-distance ratio:

$$E = \frac{V}{d} \tag{6.6}$$

being E the approximated electric field, V the applied voltage and d the distance between electrodes.

Applying Equation 6.6 to the results obtained from simulation, the approximated electric field between electrodes is:

$$E = \frac{2990.4061}{1.00331} = 2980.5\ V/cm \tag{6.7}$$

This estimated value is far from being a perfect approximation to the real electric field between the electrodes. However, if considered beforehand, it can give valuable insights about the magnitude of the electric field that is generated during the IRE procedure.

One can also notice that the intensity of the generated electric field is higher near the corners of the electrodes. Electric charges tend to spread as much as possible on the surface of a conductive material, and, therefore, there will be a higher concentration of charges in the tips of the electrodes. A higher charge density also means a higher electric field outside [54].

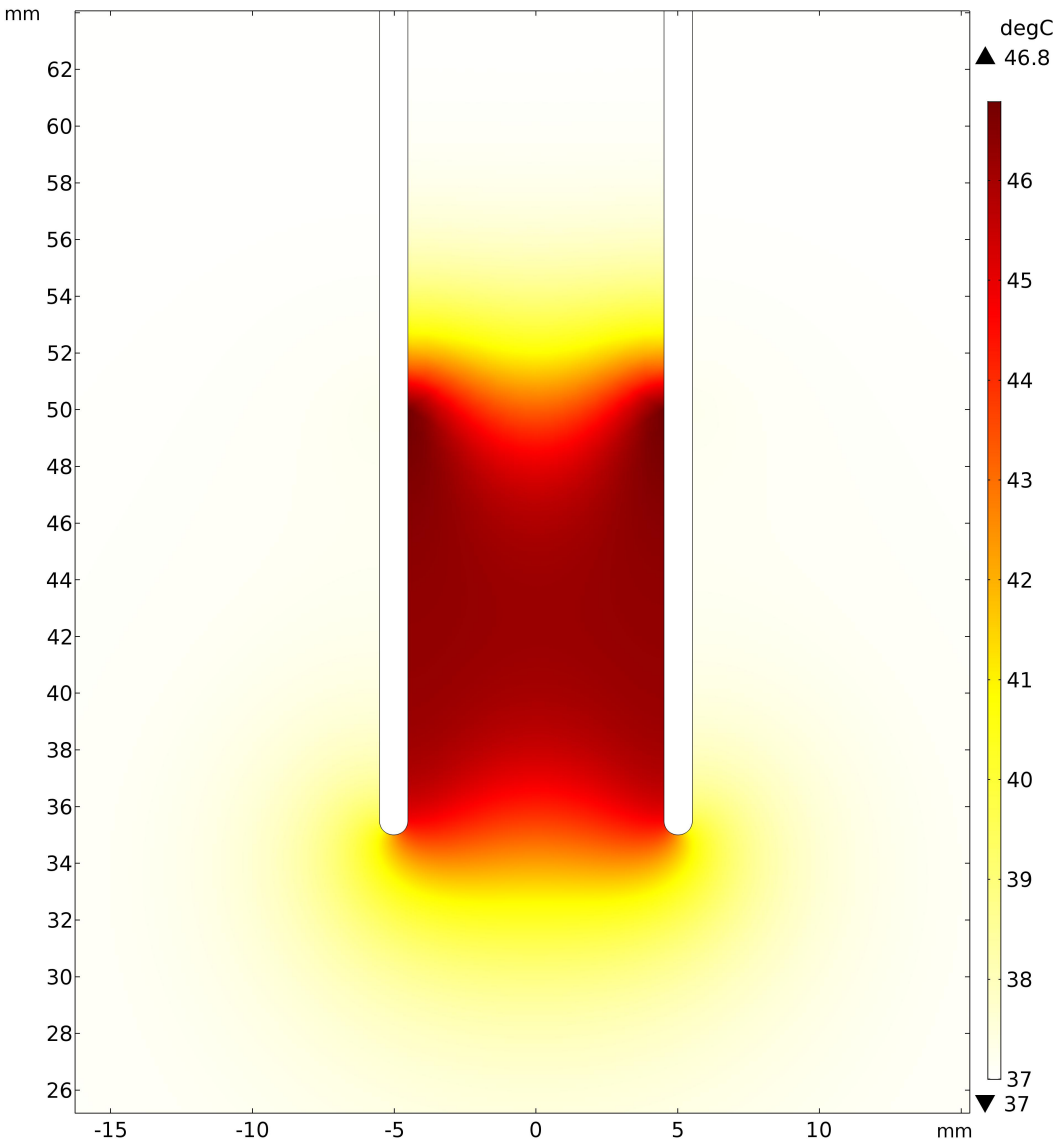

Figure 6.3: Temperature distribution in pancreatic tissue when applying the optimal IRE dose

Figure 6.3 shows that the temperature increase is more substantial in the area between the electrodes and that it follows a similar pattern to the electric field distribution. Here, the temperature seems to achieve its highest values near the vicinity of the electrodes and then eventually decreases with distance. The increase of temperature outside the area between the electrodes is not as pronounced as in between them. Overall, no thermal damage is expected to occur in the tissue when applying this IRE dose.

7 Discussion

7.1 Simulation Models

7.1.1 Geometry

In this study, 2D simulation models were built instead of 3D models for the sake of simplicity and computation speed. 2D models are a simplification of the real IRE setup and, therefore, they always present with an associated error. However, a 2D simplification of two needle electrodes is still considered a good approximation for the planning of IRE treatments [25]. This way, it is possible to avoid the simulation of 3D models which are more complex and computationally expensive.

The 2D plane considered to represent the experimental setup consisted in a cross-section perpendicular to the electrodes along the z-axis. Models in this plane represent the worst-case scenario. As a result, and for the purpose of this study, a 2D simplification would still provide reliable results.

Nevertheless, a 3D model would still be a more accurate representation of the technique. 3D models would be convenient if one would like to investigate, for instance, the ablation volume of cells after an IRE procedure.

7.1.2 FEM

A simple way to optimize the generated meshes could be done by trial, by changing their resolution and comparing the results obtained with models of different meshes [40]. If the results obtained from a model with a coarser mesh would be similar to the ones obtained by a model with a finer mesh, then it would not be necessary to apply the finer resolution mesh. This way, some computational time during simulation could be saved.

In this study, the optimization of the meshes was not investigated. Nevertheless, the meshes of the designed 2D models were created automatically by COMSOL by selecting the finest option provided by the software. The computation time was relatively fast, taking only a few minutes to simulate. This fast computation time is also related to the simplicity of the designed geometry of the models.

The mesh can also be defined by the user instead of being automatically generated. By defining finer meshes in the areas of interest and coarser meshes in the areas where the measured variables are not expected to change, some computation time might be saved. This is important, for instance, in models that are more computationally expensive, like three-dimensional models.

7.2 Design of Experiments

7.2.1 IRE Parameters

The levels of each parameter were defined taking into account the protocols that are usually used in clinical practice. However, some of the designed experiments present a combination of parameters that are not representative of an IRE treatment. For instance, in experiments 7 and 15, an applied voltage of 500 V combined with a distance between electrodes of 20 mm results in a voltage-to-distance ratio of 250 V/cm. This value is below the electric field threshold of IRE (usually around 700 V/cm). However, the main goal of this study was to calculate the optimal IRE dose. To achieve that it is necessary to collect enough data from different combinations of

parameters. In addition, the optimal IRE Dose found in this study presents a combination of parameters that make sense to be applied in a clinical point of view.

Apart from the five parameters investigated in this study, there are other parameters that can also be investigated. One of them is the implementation of breaks between pulses. There is evidence that rest periods between sequences of pulses can contribute for a decrease of temperature in the tissue, increasing the probability of cell death as well [5]. This can be an important parameter to be considered for optimization regarding the thermal effects of IRE.

Another parameter that is worth to be studied is the shape of the delivered pulses. The Gemini X2 electroporator has an extra feature that allows the delivery of exponential pulses. It would be interesting to assess the temperature outcomes from the application of these pulses and compare the outcomes with the ones obtained from the delivery of square pulses.

7.2.2 Experimental Setup

The devices used in the experimental setup allowed to replicate IRE treatments in the lab. However, some limitations of the setup can be pointed out.

The Gemini X2 electroporator is capable of delivering up to 99 pulses during a protocol. For the designed experiments in this study, the maximum number of delivered pulses was 90. However, this can be a limitation if one would like to investigate the effects delivering a larger number of pulses in a single pulse train.

The measurements of the pulse width were made by the Gemini Electroporator at the moment of their generation. Still, there might be some attenuation of the signal until the pulses reach the active part of the electrodes inserted in the target tissue. Therefore, measurements of the pulse width using the signal provided by the high-voltage probe would be more accurate. However, the resolution of the digital oscilloscope used in the experimental setup was not high enough to produce trustworthy results regarding the duration of the pulses. With a faster acquisition system the accuracy of the measurements of this parameter could be improved.

Furthermore, the temperature measurements were performed using two different measurement systems: fiber-optic temperature measurement probes and a thermocouple. The fiber-optic system was used to measure the temperature in the region between electrodes where electric fields were generated. The point measurement outside the electrodes was done using the thermocouple. Using the same temperature measurement system for the three point measurements would provide a more accurate comparison of results. In this case, it is suggested to use the fiber-optic system for all the temperature measurements since it can be applied in areas with electric fields of high magnitude.

The calibration of the temperature probes can also be done in a more efficient way. There are devices designed specifically for this purpose. For instance, calibration baths can provide temperature controlled environments for thermometer calibration. This could also improve the accuracy of the temperature results.

In addition, it was assured that the electrodes were placed parallel to each other. However, a possible misalignment of the electrodes, even if slight, might have introduced some errors in the results. This misalignment changes the electric field distribution in the tissue and, consequently, the temperature outcomes.

7.3 Temperature Results

7.3.1 Failure of Experiments 3 and 12

In experiments 3 and 12 the applied voltage of 3000 V would result in a high voltage-to-distance ratio of 6000 V/cm, which predicts the generation of very high electric fields between the inserted electrodes. In addition, there is usually a decrease of the resistance during the IRE treatment due to the changes induced by the electrical field in the target tissue [55]. Consequently, and as stated by Ohm's Law ($V = IR$), the generated current was too high to perform the experiments. Electroporators such as the Gemini X2 usually have a current limitation implemented in their system in order to avoid injuries to the patient and failure of the device. Therefore, the current that was generated during the pulse delivery was too high and the Gemini had to stop the experiment before it was completed.

7.3.2 Statistical Analysis

The ANOVA test performed with the 18 designed combination of parameters did not find any significance regarding the influence of the studied parameters in the temperature response. With a larger number of experiments more data could be collected and the results could be improved. Likewise, the validated combinations of parameters were simulated by trying different experiment durations and, therefore, the sample size was increased.

The active length was tested only in two different levels. Increasing this number to three levels, as designed for the other tested parameters, more data about this parameter would be gathered and, perhaps, the significance of the active length on the temperature could increase.

The ANOVA test showed that the voltage and the distance between the electrodes are significant parameters regarding the temperature outcomes. In fact, if the temperature results obtained from the experiments are interpreted having the voltage-to-distance ratios in mind one will find that higher voltage-to-distance ratios translate into higher temperatures in the tissue. Being the voltage-to-distance ratio an approximation to the magnitude of the generated electric field, the previous statement meets the expected: that higher magnitudes of electric field produce a higher increase in temperature. The pulse width also showed significance. Actually, the longer the pulse is "on", the more the temperature is supposed to rise in the tissue.

7.3.3 Sources of Error

The validation of the models was based on point temperature measurements. Some of the measurements presented significant differences between the results obtained in the experiments and by simulation. A possible source of error might be related to the insertion of the temperature probes in a wrong place.

The bovine liver tissue has the disadvantage of not being a transparent material. This lack of visual information makes it difficult to make sure that the temperature probes were positioned at the correct locations. Nevertheless, the probes were marked in order to be inserted at the right depths. Furthermore, the experimental setup included tubes through which the probes were inserted in order to guarantee that they were placed at the correct position in the bovine liver tissue.

From the simulation models it is possible to draw a vertical line across the bovine liver tissue to investigate the expected temperature distribution along that line. It provides information on how the temperature changes according to the insertion depth.

The first trial of experiment 5 can be taken as an illustrative example of what was previously described. The parameters that were tested in this experiment are presented in Table 7.1.

Distance Between Electrodes (mm)	**Active Length (mm)**	**Applied Voltage (V)**	**Pulse Repetitions**	**Pulse Width (µs)**
10	10	1551	80	106

Table 7.1: Parameters tested in experiment 5 (Trial 1)

Taking the vertical line that includes the center point between the electrodes it is possible to assess the distribution of the temperature according to the insertion depth. This cut line is represented in Figure 7.1.

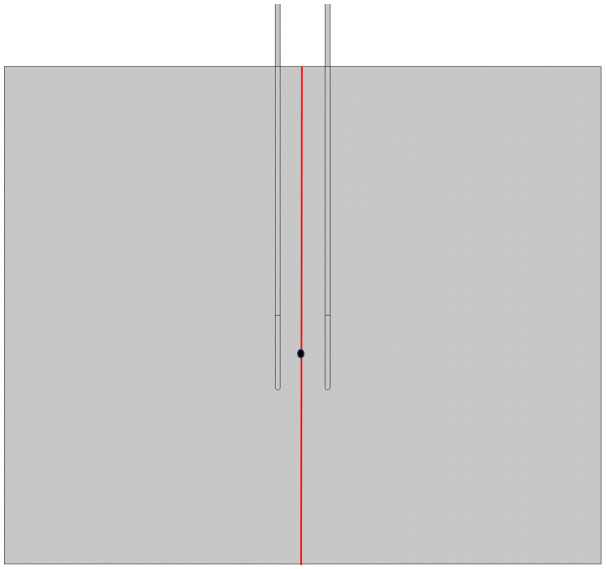

Figure 7.1: Cut line at the center point between electrodes

The red line of Figure 7.1 represents the vertical cut line. The black dot represents the center point between the electrodes where the fiber-optic probe should be inserted to measure the temperature. Figure 7.2 presents the temperature distribution along a portion of the vertical line according to the parameters of experiment 5.

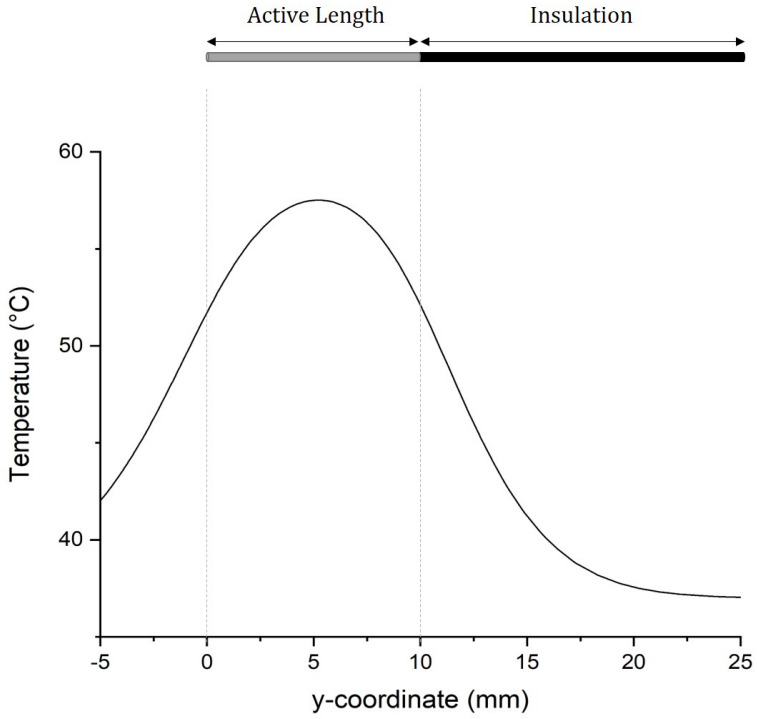

Figure 7.2: Experiment 5, Trial 1: Temperature distribution along the vertical cut line

A y-coordinate of 0 mm represents the point of the vertical line that is aligned with the tip of the electrodes. y-coordinate values between 0 and 10 mm correspond to the portion of the vertical line that is aligned with the active part of the electrodes. As a result, the center measurement point is located at the y-coordinate of 5 mm.

Figure 7.2 shows that the temperature distribution along the vertical line is not constant. As expected, the temperature increases when the y-coordinate is related to the active part of the electrodes. When, the temperature tends to decrease and stabilize at 37°C.

The maximum experimental temperature measured at the center point between the electrodes was 42.5°C. However, from the simulation models, the temperature was expected to reach a maximum temperature of 57.5°C. The temperature distribution graph shows that the measured experimental value of 42.5°C is located some millimeters away from the center point. Consequently, during the experiment, the probe might have been inserted either deeper than the defined center point between the electrodes, or not so deep and aligned with the insulated part of the electrodes.

These distribution graphs can also explain a certain trend verified in the temperature measurements where a great number of temperature results obtained by simulation presented higher values than the experimental ones.

7.4 Validation of the Models

The simulation models were validated by point measurements of temperature. However, there is another important response of the IRE technique that is worth to be investigated experimentally: the electric field.

An analytical calculation of the electric field could be used if one would like to predict the generated electric field between the electrodes beforehand. The voltage-to-distance ratio can provide an approximation of the electric field magnitude and it is useful to predict the generated

electric field according to the IRE parameters that would be tested. Nonetheless, its formula holds for the field of an infinitely large parallel plate capacitor, and therefore, it is not a good representation of the designed setup considered in this study, where two needle electrodes were inserted in the biological tissue. In this case, a more complex analytical calculation should be taken, considering the cylindrical geometry of the electrodes.

The validation of the simulation models could be improved by validating them through experimental measurements of the electric field. To do this, a device capable of directly measure the magnitude of the generated electric field would be required. This device would be inserted in the soft tissue to make point measurements of the electric field, in a similar way to the temperature measurement probes. However, one must take into account that the eventual placement of the probe between the electrodes might have influence on the electric field distribution.

7.5 IRE Optimization for Pancreatic Cancer

The validation of the simulation models in this study was made assuming that they were validated for biological tissue. Consequently, one could investigate the outcomes of an IRE treatments in a different tissue than the bovine liver tissue only by replacing the properties of this tissue by the ones of the desired biological tissue to study and then run the simulations.

The final goal of this project was to find the optimal IRE dose for pancreatic cancer. As a result, the electrical and thermophysical properties of this tissue were inserted in the models, replacing the ones of the bovine liver tissue used for the experiments. However, the electrical and thermophysical properties introduced in the models did not take into account variations with temperature. During IRE the temperature of the tissue changes and, therefore, the results obtained from simulation would be a better approximation to reality if these changes are taken into account.

Furthermore, conducting experiments in pancreatic tissue would provide more information about the validity of the models for the treatment of pancreatic cancer and it would help verifying the assumption that the models were validated for biological tissue.

The calculation of the volume of ablated cells would also add valuable information to the optimization process. Considering the ablation volume also as a response of an IRE procedure, results regarding the efficacy of the treatment could be improved even more. Moreover, experiments could confirm if no thermal damage occurred in the tissue using the optimal IRE dose.

8 Conclusions and Future Research

8.1 Conclusions

IRE is a relatively novel technique in the field of cancer treatment. Many studies have proven the potential of IRE on cancer ablation. However, there are still some skepticism about using this technique as first choice, mainly due to undefined guidelines and some uncertainty about the ideal IRE protocols that should be applied to a specific treatment.

The optimization of the applied IRE doses can help establishing well-defined treatment planning protocols. This study presented a statistically-based approach to calculate optimal IRE doses taking into account the thermal effects that result from the application of this treatment.

First, several IRE parameters that influence the outcomes of an IRE treatment were tested experimentally in a bovine liver tissue: the active length of the electrodes, the distance between the electrodes, the number of applied pulses, the width of the pulses and their voltage.

At the same time, 2D simulation models were designed and validated through experiments. Validation was done taking into account the different setups designed, with different distances between the inserted electrodes. The validation was achieved for distances between 10 and 20 mm, where great part of the experiments presented percentage errors lower than 10%.

From the validated models, it was statistically found that the distance between the electrodes ($p < 0.001$), the width of the pulses ($p = 0.002$) and the applied voltage ($p < 0.001$) had significance on the temperature outcomes of an IRE procedure.

An optimized combination of IRE parameters for the treatment of pancreatic cancer was achieved by maximizing the electric field between the electrodes while limiting the maximum temperature in the pancreatic tissue at 50°C. The optimal IRE dose found consisted in the insertion of two needle electrodes with active length of 15 mm and separated by a distance 10.0331 mm, and the delivery of 50 pulses with a width of 40.5367 µs and amplitude of 2990.4061 V. The optimal IRE dose was found taking into consideration the thermal effects in the pancreatic tissue during and IRE procedure and by trying to maximize the electric field in order to achieve the maximum possible efficacy of the treatment. An electric field magnitude of 3296.1 V/cm and a maximum temperature of 46.796°C were the measured responses when applying the optimal IRE dose to pancreatic tissue. As a result, no thermal damage in pancreatic tissue is expected to occur after applying an IRE treatment with the calculated optimal dose.

Summing up, an optimal IRE Dose that maximizes the efficacy of the treatment of pancreatic cancer was successfully calculated in this study and it can be applied with no risk of thermal damage to the tissue. Thus, the approach taken in this study can be also be applied in the future to obtain optimal IRE doses for the treatment of other types of cancer.

Nevertheless, it would have been relevant to have included the ablation area of the tissue as a response to maximize when calculating the optimal IRE doses. This would provide more insights on how effective the IRE treatment would be. Furthermore, testing other parameters, such as the frequency of the pulse delivery, and improving the accuracy of the models may also contribute to obtain even more effective optimal IRE doses and should also be object of future research.

8.2 Future Research

To improve the accuracy and reliability of the measured IRE outcomes even more, 3D models can be designed and validated. This way, a better representation of the real phenomena can be provided. Moreover, and taking advantage of the three-dimensional models, the volume of ab-

lated tissue after an IRE procedure can be calculated. In the end, optimization of the IRE doses could be performed considering the ablation volume as a response as well. Experiments with a gelatin tissue phantom could be a good way to inspect the ablation of the cells, giving its ability to mimic soft tissue and the transparency of the material. In the beginning of this project, the use of a gelatin tissue phantom in the IRE experiments failed. However, with a different combination of ingredients, perhaps the gelatin tissue phantom might perform successfully.

In order to make the IRE treatments more specific, it would be interesting to display the optimal IRE doses according to the tumor size. Knowing the generated energy along the IRE process, it would be possible to provide clinicians with information about the total energy that is required to be applied in the IRE procedure, depending on the size of the tumor that is intended to be treated. By establishing a relation between the energy and the optimal IRE parameters it would be possible to present the optimal IRE dose per tumor size. Moreover, and to investigate IRE outcomes on tumors with different sizes, it would also be interesting to try other electrode configurations such as the number of inserted electrodes and their insertion and positioning in the biological tissue.

Enhancement approaches for IRE therapy can also be object of future investigation. A new and promising approach called High-Frequency Irreversible Electroporation (H-FIRE) was proposed by Arena et al. [56]. In this modality, bursts of bipolar pulses are delivered instead of the typical monopolar pulses [57]. It would be interesting to study the thermal effects caused by the application of these pulses in biological tissue. Furthermore, it was found that using high frequencies, muscle contractions due to the application of IRE can be minimized [56]. These contractions usually contribute to the displacement of the inserted electrodes. This way, H-FIRE may contribute to make sure that the IRE outcomes, such as the electric field, temperature or ablation volume do not diverge much from the expected.

Bibliography

[1] J-P Tasu, G Vesselle, G Herpe, J-P Richer, S Boucecbi, S Vélasco, M Carretier, B Debeane, and D Tougeron. Irreversible electroporation for locally advanced pancreatic cancer. *Diagnostic and interventional imaging*, 97(12):1297–1304, 2016.

[2] Salvatore Paiella, Giovanni Butturini, Isabella Frigerio, Roberto Salvia, Giulia Armatura, Matilde Bacchion, Martina Fontana, Enrico Martone, Claudio Bassi, et al. Safety and feasibility of irreversible electroporation (ire) in patients with locally advanced pancreatic cancer: results of a prospective study. *Digestive surgery*, 32(2):90–97, 2015.

[3] Pancreatic Cancer UK. Irreversible electroporation (nanoknife) for pancreatic cancer | pancreatic cancer uk, 2018. URL https://www.pancreaticcancer.org.uk/information-and-support/treatments-for-pancreatic-cancer/irreversible-electroporation-nanoknife-for-pancreatic-cancer.

[4] Alette Ruarus, Laurien Vroomen, Robbert Puijk, Hester Scheffer, and Martijn Meijerink. Locally advanced pancreatic cancer: a review of local ablative therapies. *Cancers*, 10(1): 16, 2018.

[5] Martijn R Meijerink, Hester J Scheffer, and Govindarajan Narayanan. *Irreversible Electroporation in Clinical Practice*. Springer, 2018.

[6] EL Latouche, RV Davalos, and RCG Martin. Modeling of irreversible electroporation treatments for the optimization of pancreatic cancer therapies. In *6th European Conference of the International Federation for Medical and Biological Engineering*, pages 801–804. Springer, 2015.

[7] Govindarajan Narayanan, Peter J Hosein, Geetika Arora, Katuzka J Barbery, Tatiana Froud, Alan S Livingstone, Dido Franceschi, Caio M Rocha Lima, and Jose Yrizarry. Percutaneous irreversible electroporation for downstaging and control of unresectable pancreatic adenocarcinoma. *Journal of Vascular and Interventional Radiology*, 23(12):1613–1621, 2012.

[8] SJE Rombouts, JA Vogel, HC Van Santvoort, KP Van Lienden, R Van Hillegersberg, ORC Busch, MGH Besselink, and IQ Molenaar. Systematic review of innovative ablative therapies for the treatment of locally advanced pancreatic cancer. *British Journal of Surgery*, 102(3):182–193, 2015.

[9] Matthew Bower, Leslie Sherwood, Yan Li, and Robert Martin. Irreversible electroporation of the pancreas: definitive local therapy without systemic effects. *Journal of surgical oncology*, 104(1):22–28, 2011.

[10] Richard Drake, A Wayne Vogl, Adam WM Mitchell, Richard Tibbitts, and Paul Richardson. *Gray's Atlas of Anatomy International Edition*. Elsevier Health Sciences, 2014.

[11] Tadej Kotnik, Peter Kramar, Gorazd Pucihar, Damijan Miklavcic, and Mounir Tarek. Cell membrane electroporation-part 1: The phenomenon. *IEEE Electrical Insulation Magazine*, 28(5):14–23, 2012.

[12] EM Dunki-Jacobs, P Philips, and RCG Martin Ii. Evaluation of thermal injury to liver, pancreas and kidney during irreversible electroporation in an in vivo experimental model. *British Journal of Surgery*, 101(9):1113–1121, 2014.

[13] Martin JC van Gemert, Peter GK Wagstaff, Daniel M de Bruin, Ton G van Leeuwen, Allard C van der Wal, Michal Heger, and Cees WM van der Geld. Irreversible electroporation: just another form of thermal therapy? *The Prostate*, 75(3):332–335, 2015.

[14] Paulo A Garcia, Rafael V Davalos, and Damijan Miklavcic. A numerical investigation of the electric and thermal cell kill distributions in electroporation-based therapies in tissue. *PloS one*, 9(8):e103083, 2014.

[15] Rafael V Davalos, LM Mir, and B Rubinsky. Tissue ablation with irreversible electroporation. *Annals of biomedical engineering*, 33(2):223, 2005.

[16] Alexander Golberg and Martin L Yarmush. Nonthermal irreversible electroporation: fundamentals, applications, and challenges. *IEEE Transactions on biomedical Engineering*, 60(3):707–714, 2013.

[17] Chunlan Jiang, Rafael V Davalos, and John C Bischof. A review of basic to clinical studies of irreversible electroporation therapy. *IEEE Transactions on biomedical Engineering*, 62 (1):4–20, 2015.

[18] Davorka Sel, David Cukjati, Danute Batiuskaite, Tomaz Slivnik, Lluis M Mir, and Damijan Miklavcic. Sequential finite element model of tissue electropermeabilization. *IEEE Transactions on Biomedical Engineering*, 52(5):816–827, 2005.

[19] Saša Haberl, D Miklavcic, G Sersa, Wolfgang Frey, and Boris Rubinsky. Cell membrane electroporation-part 2: the applications. *IEEE Electrical Insulation Magazine*, 29(1):29–37, 2013.

[20] Chenguo Yao, Shoulong Dong, Yajun Zhao, Yanpeng Lv, Hongmei Liu, Lingyu Gong, Jianhao Ma, Haifeng Wang, and Yinghao Sun. Bipolar microsecond pulses and insulated needle electrodes for reducing muscle contractions during irreversible electroporation. *IEEE Transactions on Biomedical Engineering*, 64(12):2924–2937, 2017.

[21] M Rebersek, D Miklavcic, C Bertacchini, and M Sack. Cell membrane electroporation-part 3: the equipment. *IEEE Electrical Insulation Magazine*, 30(3):8–18, 2014.

[22] Johann J Wendler, Katharina Fischbach, Jens Ricke, Julian Jürgens, Frank Fischbach, Jens Köllermann, Markus Porsch, Daniel Baumunk, Martin Schostak, Uwe-Bernd Liehr, et al. Irreversible electroporation (ire): standardization of terminology and reporting criteria for analysis and comparison. *Polish journal of radiology*, 81:54, 2016.

[23] Chunlan Jiang, Qi Shao, and John Bischof. Pulse timing during irreversible electroporation achieves enhanced destruction in a hindlimb model of cancer. *Annals of biomedical engineering*, 43(4):887–895, 2015.

[24] Chunlan Jiang, Zhenpeng Qin, and John Bischof. Membrane-targeting approaches for enhanced cancer cell destruction with irreversible electroporation. *Annals of biomedical engineering*, 42(1):193–204, 2014.

[25] Rafael V Davalos and Boris Rubinsky. Temperature considerations during irreversible electroporation. *International journal of heat and mass transfer*, 51(23-24):5617–5622, 2008.

[26] Yongji Yang, Michael Moser, Edwin Zhang, Wenjun Zhang, and Bing Zhang. Optimization of electrode configuration and pulse strength in irreversible electroporation for large ablation volumes without thermal damage. *Journal of Engineering and Science in Medical Diagnostics and Therapy*, 1(2):021002, 2018.

[27] Qi Shao, Feng Liu, Connie Chung, Kianna Elahi-Gedwillo, Paolo P Provenzano, Bruce Forsyth, and John C Bischof. Physical and chemical enhancement of and adaptive resistance to irreversible electroporation of pancreatic cancer. *Annals of biomedical engineering*, 46(1):25–36, 2018.

[28] Bing Zhang, Michael AJ Moser, Edwin M Zhang, Jim Xiang, and Wenjun Zhang. An in vitro experimental study of the pulse delivery method in irreversible electroporation. *Journal of Engineering and Science in Medical Diagnostics and Therapy*, 1(1):014501, 2018.

[29] Zhenpeng Qin, Jing Jiang, Gary Long, Bruce Lindgren, and John C Bischof. Irreversible electroporation: an in vivo study with dorsal skin fold chamber. *Annals of biomedical engineering*, 41(3):619–629, 2013.

[30] Chenguo Yao, Yanpeng Lv, Shoulong Dong, Yajun Zhao, and Hongmei Liu. Irreversible electroporation ablation area enhanced by synergistic high-and low-voltage pulses. *PloS*

one, 12(3):e0173181, 2017.

[31] Angio Dynamics. The nanoknife system - angiodynamics, 2019. URL https://www.angiodynamics.com/products/2/The-NanoKnife-System.

[32] Robert CG Martin II, Kelli McFarland, Susan Ellis, and Vic Velanovich. Irreversible electroporation therapy in the management of locally advanced pancreatic adenocarcinoma. *Journal of the American College of Surgeons*, 215(3):361–369, 2012.

[33] Robert CG Martin, Kelli McFarland, Susan Ellis, and Vic Velanovich. Irreversible electroporation in locally advanced pancreatic cancer: potential improved overall survival. *Annals of surgical oncology*, 20(3):443–449, 2013.

[34] Sandeep Bagla and Dimitrios Papadouris. Percutaneous irreversible electroporation of surgically unresectable pancreatic cancer: a case report. *Journal of Vascular and Interventional Radiology*, 23(1):142–145, 2012.

[35] Marco Cavazzuti. *Optimization methods: from theory to design scientific and technological aspects in mechanics*. Springer Science & Business Media, 2012.

[36] G Taguchi and Y Wu. Introduction to off-line quality control, central japan quality control association. *Available from American Supplier Institute*, 32100, 1980.

[37] Minitab. Taguchi designs, 2019. URL https://support.minitab.com/en-us/minitab/18/help-and-how-to/modeling-statistics/doe/supporting-topics/taguchi-designs/taguchi-designs.

[38] OMEGA Engineering. Fiber-optic temperature measurement, 2018. URL https://www.omega.com/prodinfo/fiber-optic-temperature-measurement.html.

[39] Rafael V Davalos, Paulo A Garcia, and Jon F Edd. Thermal aspects of irreversible electroporation. In *Irreversible Electroporation*, pages 123–154. Springer, 2010.

[40] Nataša Pavšelj and Damijan Miklavčič. Finite element modeling of in vivo electroporation. In *Irreversible Electroporation*, pages 183–202. Springer, 2010.

[41] Harry H Pennes. Analysis of tissue and arterial blood temperatures in the resting human forearm. *Journal of applied physiology*, 1(2):93–122, 1948.

[42] Frank P Incropera, Adrienne S Lavine, Theodore L Bergman, and David P DeWitt. *Fundamentals of heat and mass transfer*. Wiley, 2007.

[43] Xiaoming He and John C Bischof. Quantification of temperature and injury response in thermal therapy and cryosurgery. *Critical Reviews in Biomedical Engineering*, 31(5&6), 2003.

[44] Zhen Ji and Christopher L Brace. Expanded modeling of temperature-dependent dielectric properties for microwave thermal ablation. *Physics in Medicine & Biology*, 56(16):5249, 2011.

[45] Idir Mellal, Emmanuel Kengne, Karim El Guemhioui, and Ahmed Lakhssassi. 3d modeling using the finite element method for directional removal of a cancerous tumor. *J Biomedical Sci*, 5(4), 2016.

[46] Christian Rossmann and Dieter Haemmerich. Review of temperature dependence of thermal properties, dielectric properties, and perfusion of biological tissues at hyperthermic and ablation temperatures. *Critical Reviews in Biomedical Engineering*, 42(6), 2014.

[47] A Bhattacharya and RL Mahajan. Temperature dependence of thermal conductivity of biological tissues. *Physiological measurement*, 24(3):769, 2003.

[48] Constantin Ionescu-Tirgoviste, Paul A Gagniuc, Elvira Gubceac, Liliana Mardare, Irinel Popescu, Simona Dima, and Manuella Militaru. A 3d map of the islet routes throughout the healthy human pancreas. *Scientific reports*, 5:14634, 2015.

[49] PA Hasgall, E Neufeld, MC Gosselin, A Klingenböck, and N Kuster. It'is database for thermal and electromagnetic parameters of biological tissues. *Version 4.0*, 2018.

[50] Rajnish Sharma and Raji Sundararajan. Electric field distribution study of pancreatic tumors. *Journal of Cancer Prevention and Current Research*, 8, 12 2017. doi: 10.15406/jcpcr.2017.08.00303.

[51] Minitab. Response surface designs, 2019. URL https://support.minitab.com/en-us/minitab/18/help-and-how-to/modeling-statistics/doe/supporting-topics/response-surface-designs/response-surface-central-composite-and-box-behnken-designs.

[52] Minitab. Individual desirabilities, 2019. URL https://support.minitab.com/en-us/minitab/18/help-and-how-to/modeling-statistics/using-fitted-models/how-to/response-optimizer/methods-and-formulas/individual-desirabilities.

[53] Minitab. Composite desirability, 2019. URL https://support.minitab.com/en-us/minitab/18/help-and-how-to/modeling-statistics/using-fitted-models/how-to/response-optimizer/methods-and-formulas/individual-desirabilities.

[54] Richard P Feynman, Robert B Leighton, and Matthew Sands. *The Feynman lectures on physics, Vol. I: The new millennium edition: mainly mechanics, radiation, and heat*, volume 1. Basic books, 2011.

[55] Claudio Bertacchini, Pier Mauro Margotti, Enrico Bergamini, Mattia Ronchetti, and Ruggero Cadossi. Irreversible electroporation systems for clinical use. In *Irreversible electroporation*, pages 255–272. Springer, 2010.

[56] Christopher B Arena, Michael B Sano, John H Rossmeisl, John L Caldwell, Paulo A Garcia, Marissa Nichole Rylander, and Rafael V Davalos. High-frequency irreversible electroporation (h-fire) for non-thermal ablation without muscle contraction. *Biomedical engineering online*, 10(1):102, 2011.

[57] Michael B Sano, Christopher B Arena, Katelyn R Bittleman, Matthew R DeWitt, Hyung J Cho, Christopher S Szot, Dieter Saur, James M Cissell, John Robertson, Yong W Lee, et al. Bursts of bipolar microsecond pulses inhibit tumor growth. *Scientific reports*, 5:14999, 2015.

[58] Mohammed Shurrab, Haidong Wang, Noriaki Kubo, Takanobu Fukunaga, Kosaku Kurata, and Hiroshi Takamatsu. The cooling performance of a cryoprobe: Establishing guidelines for the safety margins in cryosurgery. *International Journal of Refrigeration*, 67:308–318, 2016.

Appendix A: Experiments with a Gelatin Tissue Phantom

The 18 designed experiments were initially tested in a gelatin tissue phantom instead of bovine liver tissue. The tissue phantom was made of a combination of 3% Bovine Bone Gelatin (granular), 0.3% Agarose type-III and 0.9% sodium chloride powder, all mixed in deionized water [58]. With this combination of ingredients, the electrical and thermophysical properties of the gelatin tissue phantom can mimic the ones of skin tissue.

Unfortunately, it was not possible to perform experiments with this gelatin tissue phantom while delivering high voltage pulses. The Gemini X2 electroporator performs measurements of the resistive load of the target tissue before delivering the train of pulses. These measurements always revealed low values of resistance of the gelatin tissue phantom (50 - 90 Ω). As a result, the generated current during the pulse delivery was too high and the Gemini stopped the experiments as a safety procedure. Furthermore, some light sparks at the active part of the positive electrode were observed when the pulses were being delivered to the gelatin tissue phantom, before the Gemini stopped the experiment (Figure A.1). It was also possible to hear the sound of those sparks.

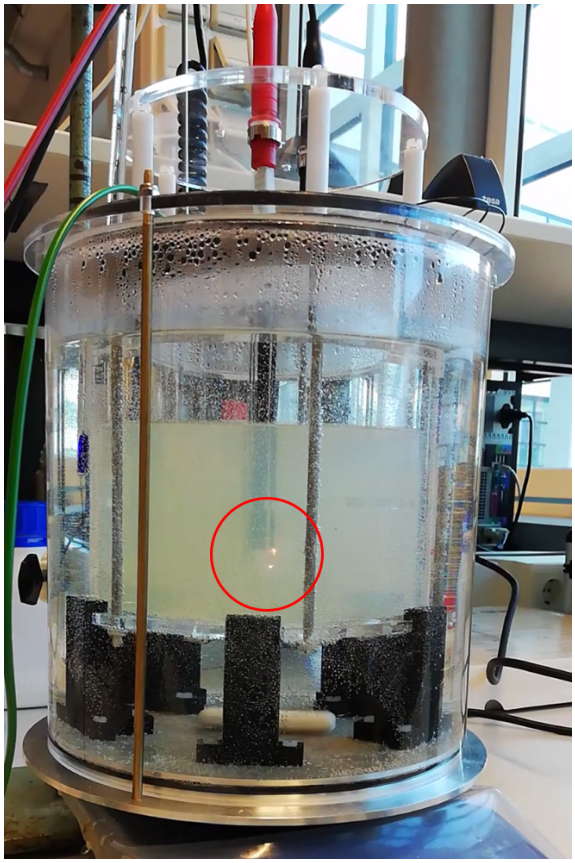

Figure A.1: Light sparks when delivering pulses to the gelatin tissue phantom

Delivery of pulses with amplitude higher than 500 V for a distance between electrodes of 10 mm and higher than 1000 V for a distance between electrodes of 20 mm was not possible to perform. These settings result in voltage-to-distance ratios of 500 V/cm, which are under the estimated IRE threshold of 700 V/cm. As a result, the experiments that were possible to be done with the gelatin tissue phantom would not be representative of IRE treatments.

Appendix B: Experimental Setup

A part of the experimental setup is presented in Figure B.1. The picture includes the inner container with bovine liver tissue, fixed inside the thermostatic bath placed on the hot plate. The yellow wires are the fiber-optic temperature measurement probes, while one of the green cables connected the thermocouple to a digital thermometer. The electrodes were connected to the Gemini X2 electroporator via HV cables (black and red cables).

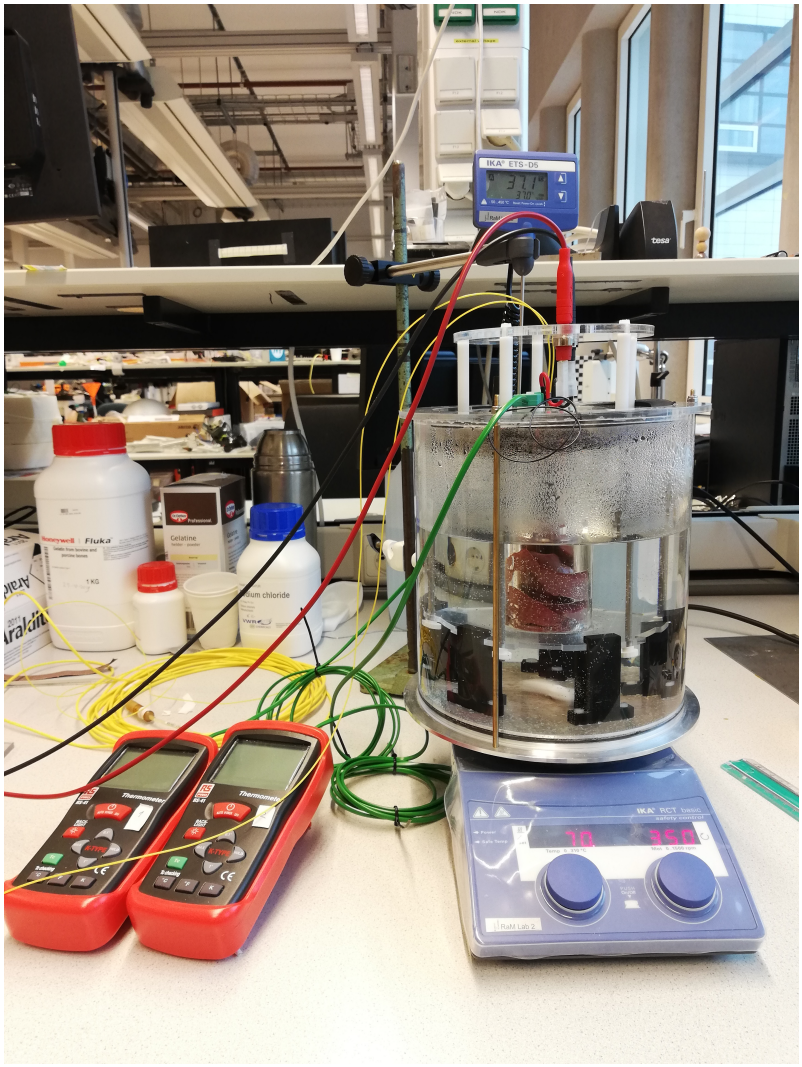

Figure B.1: Experimental Setup

The top plates of the cylindrical container where the bovine liver tissue was inserted are presented in Figure B.2, Figure B.3 and Figure B.4, for distances between electrodes of 5 mm, 10 mm and 20 mm, respectively. Between the electrodes it is possible to see the tubes that supported the insertion of the fiber-optic temperature measurement probes.

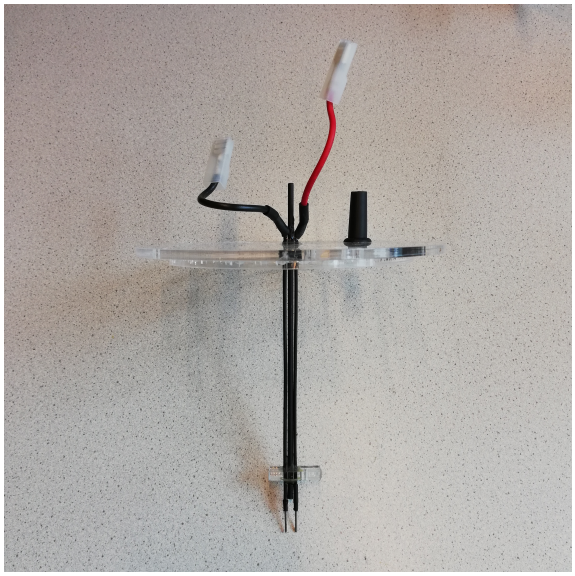

Figure B.2: Top plate for a distance between electrodes of 5 mm

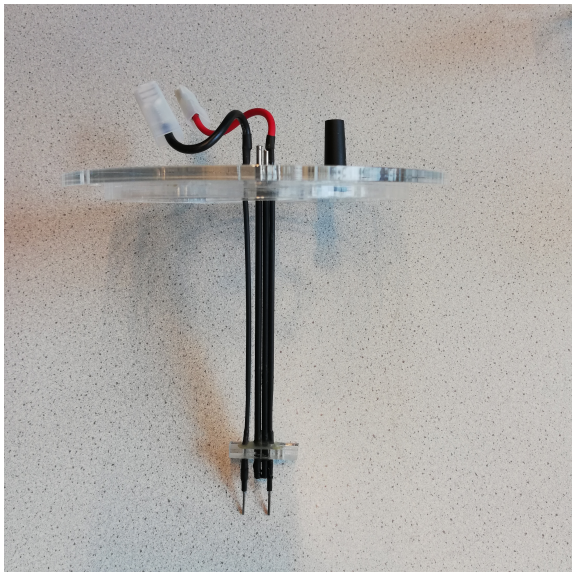

Figure B.3: Top plate for a distance between electrodes of 10 mm

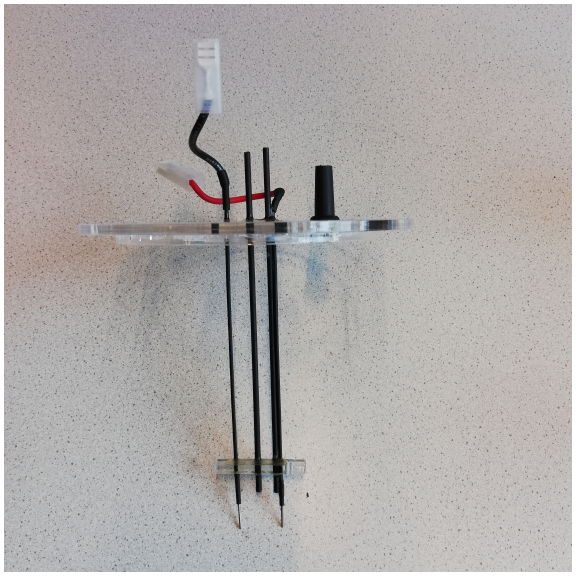

Figure B.4: Top plate for a distance between electrodes of 20 mm